Design of Surface-Modified Anode Materials with High Electrical Conductivity for High-Performance Lithium-Ion Batteries

Seunghee Ko

Department of Energy Engineering
(Battery Science and Technology)

Graduate school of UNIST

2015

Design of Surface-Modified Anode Materials with High Electrical Conductivity for High-Performance Lithium-Ion Batteries

Seunghee Ko

Department of Energy Engineering
(Battery Science and Technology)

Graduate school of UNIST

Design of Surface-Modified Anode Materials with High Electrical Conductivity for High-Performance Lithium-Ion Batteries

A dissertation
submitted to the Graduate School of UNIST
in partial fulfillment of the
requirements for the degree of
Master of Science.

Seunghee Ko

12. 16. 2014
Approved by

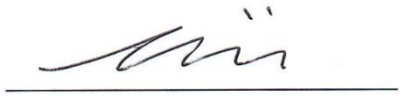

Advisor
Soojin Park

Design of Surface-Modified Anode Materials with High Electrical Conductivity for High-Performance Lithium-Ion Batteries

Seunghee Ko

This certifies that the dissertation of Seunghee Ko is approved.

12. 16. 2014

Advisor: Soojin Park

Sang-Young Lee

Byeong-Su Kim

Abstract

In the past decades, sustainable and clean energy have been demanded because of a serious exhaustion of resources and environmental problems. For this reason, many researchers have tried to develop more efficient and powerful energy devices. Among them, lithium ion batteries (LIBs) have been considered the most promising energy storage devices, because they can exhibit high power and high energy densities that meet the requirements for hybrid electric vehicles (HEVs) and electric vehicles (EVs) applications. However, although LIBs have been successfully commercialized, a considerable improvement of anode materials is still required for large scale energy storage applications and advanced future electronic devices.

Natural graphite anode in LIBs shows very small volume change (~10 % at high temperature), a stable cycling life, a low reaction potential (vs. Li/Li^+) and a low cost. These factors satisfy the requirements for commercialization as LIB anodes. However, limited specific capacity (372 mAh g^{-1}) of graphite hinders its usage to high-energy density applications. For this reason, alternative anode materials which can exhibit a high specific capacity at a low reaction potential have been studied. Silicon (Si) is one of the most promising candidates for the next -generation anode material due to its high theoretical specific capacity (>3500 mAh g^{-1} at room temperature), low lithiation potential (<0.5 V vs. Li/Li^+), low cost, and environmental safety. However, Si anode should solve two major problems to replace graphite anode in commercial LIBs. One is a large volume changes (>300%) upon insertion and extraction of lithium ions, leading to the pulverization and significant capacity fading. The other is a low intrinsic electrical conductivity. To overcome these critical obstacles, various strategies have been developed including design of novel structures, reduction of particle size, and combination of active materials and other materials having excellent electrical conductivity.

In this study, we introduced nanomaterials with high electrical conductivity (e.g., silver, antimony-doped tin oxide, etc.) on the surface of Si and graphite. These newly-developed anode materials exhibited significantly improved electrochemical properties, compared to bare Si or graphite anode materials. These simple, but straightforward synthetic routes can be extended to make other advanced anode materials for high-performance LIBs.

Contents

List of figures

Figure 3.7. Elemental analysis (EA) of ATO-NG. The amount of ATO colloidal solution was fixed to 0.5 g: Without carbon coating using (a) non-activated graphite and (b) activated-graphite, and with carbon coating using (c) non-activated graphite and (d) activated graphite.

Figure 3.8. Electrochemical performances of bare natural graphite and ATO-coated graphite electrodes: (a) First cycle at 0.05 C in the range of 0.005-3 V and (b) cycling performance of bare natural graphite and ATO-coated graphite electrodes.

Figure 3.9. Rate capabilities (0.2-5 C) of bare natural graphite and ATO-NG electrodes.

List of tables

I. Introduction

1.1 Principle of lithium ion batteries

In these days, energy problems have been seriously raised because of the depletion of fossil fuels, so that the development of sustainable and renewable energy resources should be necessary. For this reason, applications of energy storage devices have attracted much attention.[1-2] There are many types of energy storage devices, such as lead-acid battery, Na-S battery, flow batteries, supercapacitors, and lithium ion batteries (LIBs).[3] Among them, LIBs are one of the attractive storage devices owing to their high energy density, long cycle life and economic considerations. First commercialized LIBs was developed in 1991 by Sony Co.[4] Although LIBs have been successfully commercialized, a noticeable improvement about the energy densities should be necessary to meet the requirements for the applications such as electric vehicles (EVs), or energy storage systems (ESS).[5-6] Therefore, many advanced developments for LIBs have to be performed.

The principle of LIBs is shown in Figure 1.2.a. During the discharge, an anode donates electrons and a cathode accepts electrons, while electrolyte allows the low of lithium ions and separator blocks the electronic flow between the anode and the cathode. The electrochemical reaction at all electrodes during the discharge and the charge can be explained through the following equations.[7]

$$\text{Cathode: } LiCoO_2 \rightleftarrows Li_{1-x}CoO_2 + xLi^+ + xe^-$$
$$\text{Anode: } C_6 + xLi^+ + xe^- \rightleftarrows Li_xC_6$$
$$\text{Total reaction: } LiCoO_2 + C_6 \rightleftarrows Li_{1-x}CoO_2 + Li_xC_6$$

The driving force of LIBs is potential difference between anode and cathode (Figure 1.2.b). To increase energy density, cathode materials should have higher potential and anode should have lower potential. The amount of ions which inserts into electrodes determines a specific capacity of electrical storage devices. It indicates that the types of ions and materials are main factors that influence the amount of electric energy to be stored.[8]

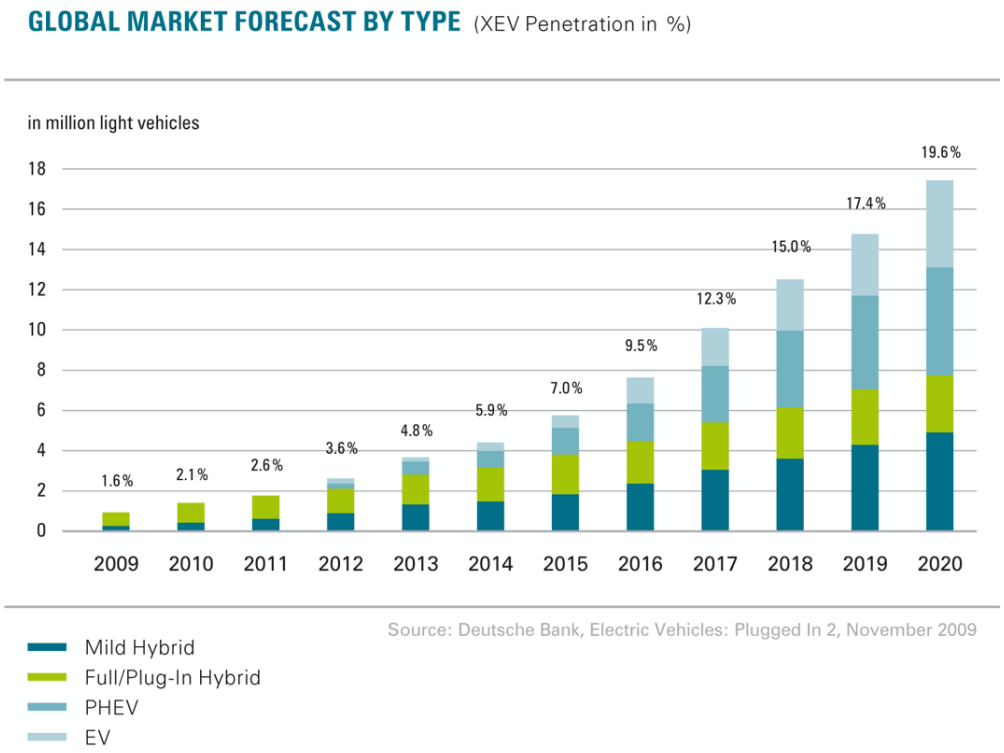

Figure 1.1. Global LIBs market status and forecast (2009~2020). The demand of LIBs will be increased explosively.[9]

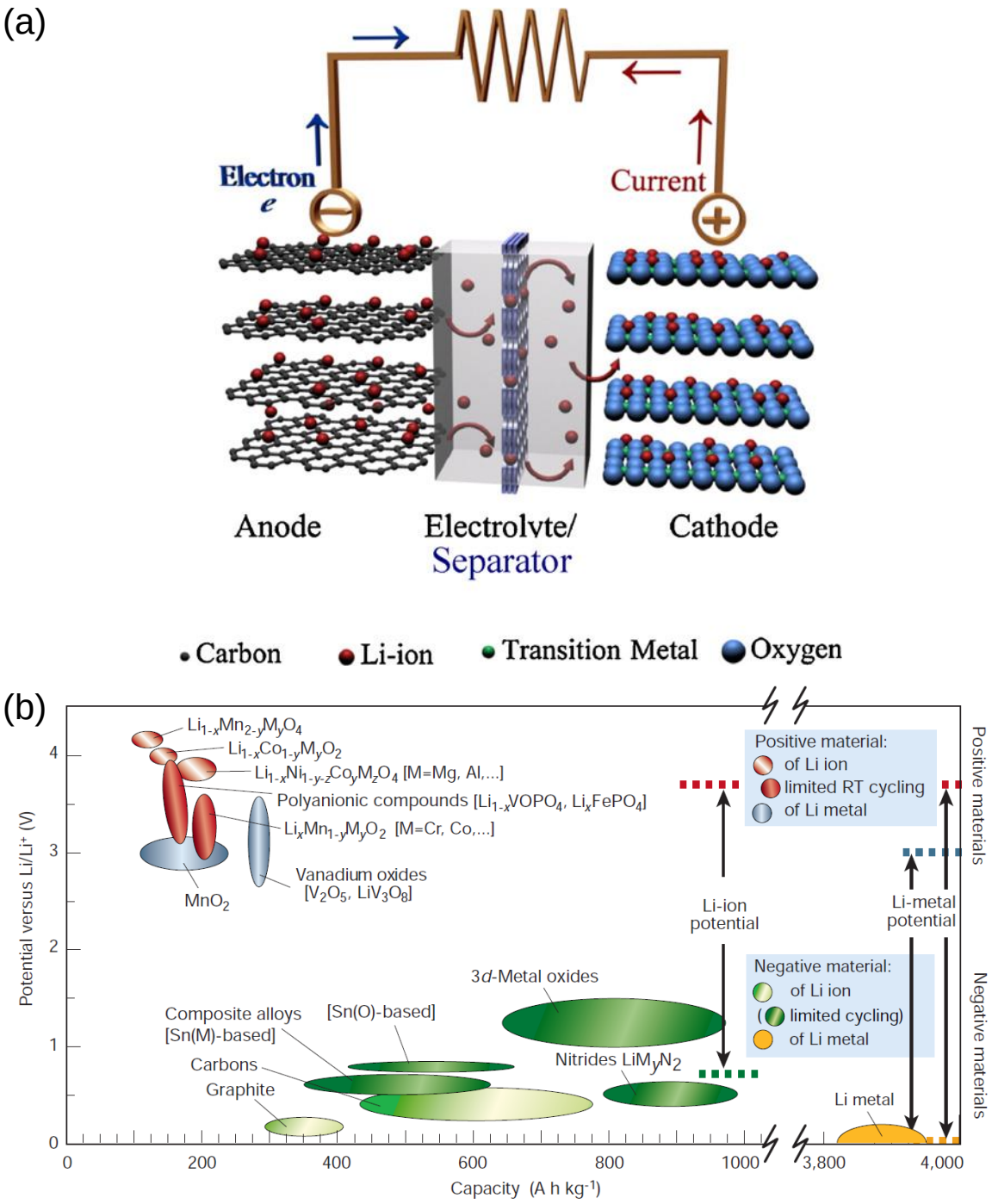

Figure 1.2. (a) Schematic illustration of typical LIBs where $LiCoO_2$ and graphite are used as the cathode and the anode, respectively[10], (b) potential versus capacity for cathode and anode electrodes presently used or under serious considerations for the rechargeable Li-based cells.[8]

1.2 Components of lithium ion batteries

LIBs are composed of four parts including cathodes, anodes, separators and electrolytes. The specific usable materials of each components in the LIBs are shown in Table 1.1.[11] Cathode materials commonly used are lithium transition metal oxides that have layered structure with the formula of $LiMO_2$ (M = Mn, Co, and Ni) and spinel LiM_2O_4, and lithium transition metal phosphates such as olivine $LiMPO_4$. Cathode materials have been developed by surface coating, mixing, or compound formation to minimize some side reactions occurring on the cathode surface.[12]

In general, carbonaceous material (e.g., graphite) has been used as an anode material for LIBs, which has a theoretical capacity of 372 mAh g^{-1}. Its specific capacity is not sufficient for the application of large scale energy storage devices. To realize the high energy and power density, Li alloy-based materials (Si, Al, Sn, Sb, Ge, etc) are considered as the alternatives. However, critical problems are a large volume expansion and formation of unstable solid electrolyte interphase (SEI) layers during cycling and should be solved to use in practical LIBs.[7] Electrolyte is a medium for transporting solvated lithium ions between both electrodes during electrochemical processes and separator, keep an anode apart from a cathode physically and prevent the electronic current, but allow the lithium ions flow.[5] The appropriate conditions for electrolyte and separator are fastidious, so, many researches have been tried in order to meet the complicated situations.

Table 1.1. Specific examples of major components in a LIBs.[11]

Component	Materials
Cathode	Transition metal oxide/phosphate: $LiCoO_2$, $LiMn_2O_4$, $LiNiO_2$, $LiFePO_4$
Anode	Carbon/noncarbon materials: graphite, hard (soft) carbon, Li, Si, Sn, Ge.
Separator	Polymer: polyethylene (PE), polypropylene (PP) , PVdF
Electrolyte	Nonaqueous organic solvent + lithium salt + additives

1.2.1 Cathode materials

The most popular cathode materials are based on transition metal oxides, which enables the intercalation/de-intercalation of lithium ions between the close packed transition metal-oxygen layers with the formula of $LiMO_2$ (M = Co, Mn, and Ni).[12]

The first commercialized cathode material is $LiCoO_2$ with the theoretical capacity of 274 mAh g^{-1}, and it reacts with lithium ions around 4 V.[13] However, $LiCoO_2$ has a serious reversibility problem: the extraction of lithium ions from Li_xCoO2 ($x<0.5$) causes the limiting capacity to 160 mAh g^{-1}.[13-14] And it leads the irreversible structural change at the lithium ion deficient phases. Moreover, a toxicity, a poor safety and a high cost of cobalt limit the application for the large scale energy storage. To improve the electrochemical performances of $LiCoO_2$, metal oxides (ZrO_2, Al_2O_3, MgO, and SnO_2) coating on the $LiCoO_2$ surface or doping with the trivalent ions (Al and Cr) can be applied.[14-16]

$LiNiO_2$ is considered as alternative cathode to $LiCoO_2$. $LiNiO_2$ has a higher specific capacity of 200 mAh g^{-1} compared to the specific capacity of $LiCoO_2$.[17] However, $LiNiO_2$ shows a serious capacity fading during cycling and the collapse of delithiated Li_xNiO_2.[18] For this reason, the formation of $LiNi_{1-x}Co_xO_2$ via the substitution of Co for Ni is tired.[17, 19] $LiMnO_2$ is also considered as the alternative because if the high thermal stability, but its applications is limited because of the low specific capacity.[20]

The other representative cathode material is $LiMn_2O_4$ with spinel structure. It is highlighted for the EVs and HEVs application due to their high power density, high thermal stability and low cost. However, $LiMn_2O_4$ has two major problems, one is the dissolution of manganese ions (Mn^{2+}) at the elevated temperature. When Mn^{2+} dissolved in the electrolytes and moved to the anode, manganese ions deposit at the anode and inhibit the movement of lithium ions, thus the capacity fading occurs during cycling. The other problem is the irreversible structural transition by Jahn-Teller distortion. However, above all things, a low capacity (130mAh g^{-1}) is the most critical problem of $LiMn_2O_4$.[21-22]

Furthermore, many researchers have studied $LiFePO_4$, which is one of the most prominent material for large scale storage applications. $LiFePO_4$ with olivine structure has many advantages such as low cost of Fe, high theoretical capacity of 170 mAh g^{-1}, excellent cycle life, and high safety. But its low electronic conductivity and low lithium ion diffusion rate should be needed to improve.[23]

Generally, each cathode materials have similar problems that affect to long cycle life or high rate capability. These are caused by the structural deterioration. For example, when transition metal moved toward lithium site, it blocks the pathways of lithium ions, so that cycle retention or high rate performance is decreased. Also, cations react with electrolyte during charge and discharge, and the electrolyte with organic compounds is decomposed. As a result, by-products produced on the cathode material surface, and interrupt the diffusion of lithium ions and electron transfer. These problems can be solved various methods, such as coating, doping on the surface of cathode materials or downsizing of materials.

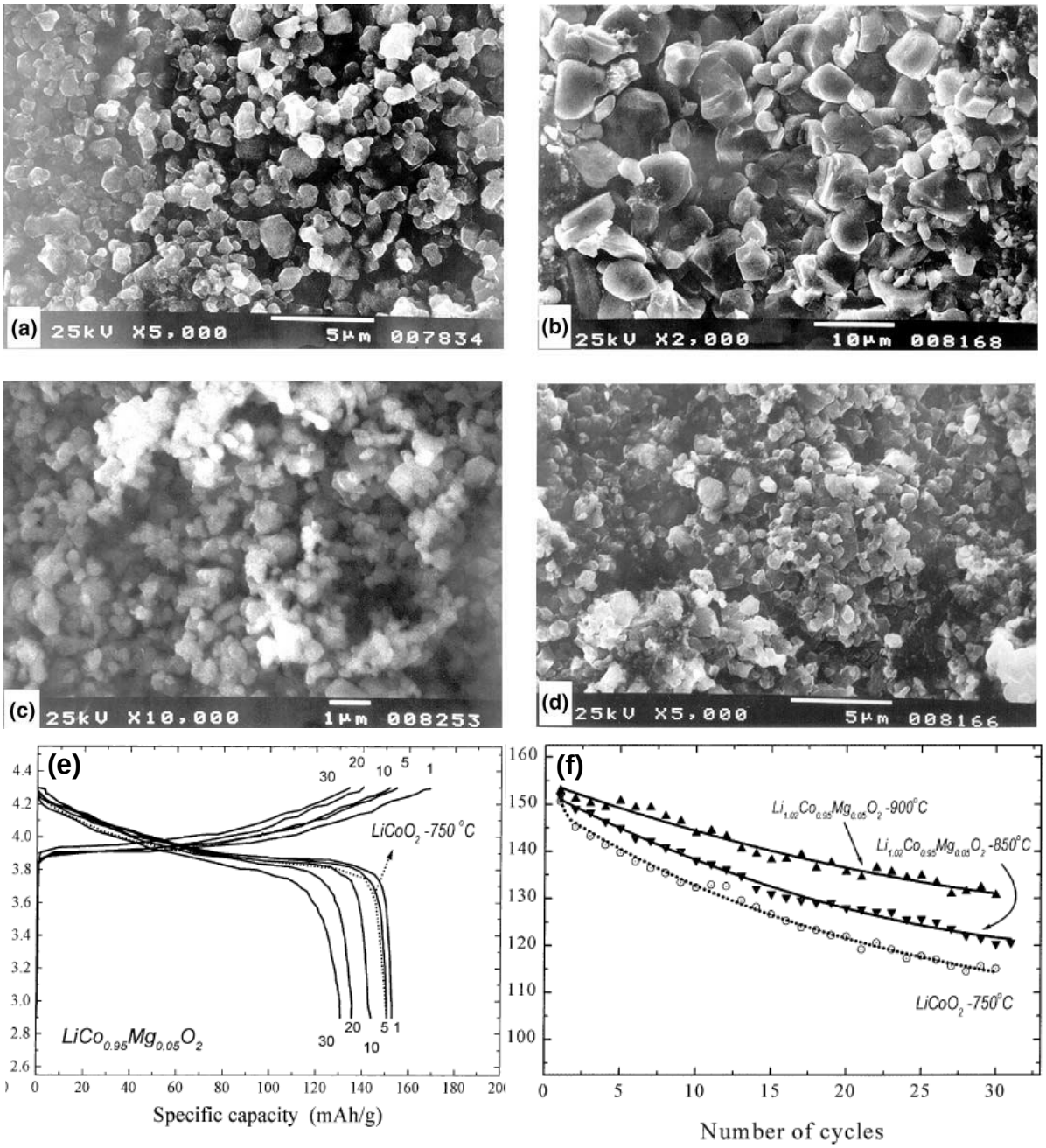

Figure 1.3. SEM images of pure $LiCoO_2$ prepared at (a) 750 ºC and (b) 900 ºC, SEM images of Mg-doped $LiCoO_2$ prepared at (c) 850 ºC and (d) 900 ºC, (e) charge/discharge curves until 30th cycles and (f) cycling performance of $LiCoO_2$ and Mg-doped $LiCoO_2$.[24]

1.2.2 Anode materials

In the early stage of development in LIBs, lithium metal has been widely used as an anode material because of its high theoretical capacity (~3860 mAh g^{-1}) and very low standard redox potential (-3.04V vs. SHE). However, lithium metal has serious problems: one is the dendrite formation during insertion and extraction of lithium ions, leading to short circuit and explosion. And the other is a low coulombic efficiency by the growth of unstable SEI layer.[8] In order to overcome the disadvantages, many studies have been tried to replace lithium metal.

Among many candidates of the anode materials for LIBs, carbonaceous materials have received much attention. In particular, graphite is representative material that reacts with lithium ions by the intercalation/deintercalation reaction, and is very close to the lithium metal potential of electrochemical reaction (<0.2V vs. Li/Li^+). Also, it indicates a low irreversibility capacity and low cost. But a low theoretical capacity of 372 mA h g^{-1} is not suitable for the demand of market.[7, 25] Therefore, it is necessary to develop new materials to increase specific capacity for the large scale application.

As alternative materials to the graphite, lithium alloying materials have been developed, such as Si, Sn, Ge, Al, and Ag.[26] Lithium ions react with them through the alloy/de-alloying process and those have much higher specific capacity compared to the graphite. Among them, silicon (Si) is the most promising material because of its high theoretical capacity (>3500 mAh g^{-1} at room temperature) and a low lithiation potential (<0.4V vs. Li/Li^+).[27] However, the chronic problems, a large volume change (>300%) during cycling, which leads to pulverization and subsequent formation of unstable SEI layer.[28] These problems were prevented through a morphology control (nanowires, nanotubes, porous structure, or hollow structure)[29-30], a surface modification (carbon, metal, or polymer coating)[31], and a formation of multiphase composites.[32]

Metal oxides have been also studied as the anode materials for LIBs. Unlike others, each metal oxide has different reaction with lithium ions. For example, tin oxide (SnO_2) reacts with lithium ions by alloy mechanism, and TiO_2 has the insertion/extraction process. Moreover, conversion mechanism occurs in MO_x (M = Co, Fe, Cu, Ni, etc.) materials.[18, 33] The specific capacity of metal oxide is higher than the graphite, but they cannot use at the large scale application because their large irreversible initial capacity and a poor cycle life due to the Li_2O formation.[7, 33] Through a nanostructuring and a surface modification, problems of metal oxides can be improved.[33-35]

Therefore, the development of advanced anode materials which has a high specific capacity, a long cycle life, an excellent rate capability, and environmentally friendly is significantly needed for the next generation LIBs.

Table 1.2. Specific examples of anode materials in a LIBs and their characteristics.[36]

Materials	**Theoretical specific capacity (mA h g^{-1})**	**Theoretical charge density (mA h cm^{-3})**	**Potential (vs. Li/Li^+)**	**Volume change (%)**
Lithium	3862	2047	0	100
Graphite	372	837	0.05	12
$Li_4Ti_5O_{12}$	175	613	1.6	1
Si	4200	9786	0.4	320
Sn	994	7246	0.6	260
Al	993	2681	0.3	96

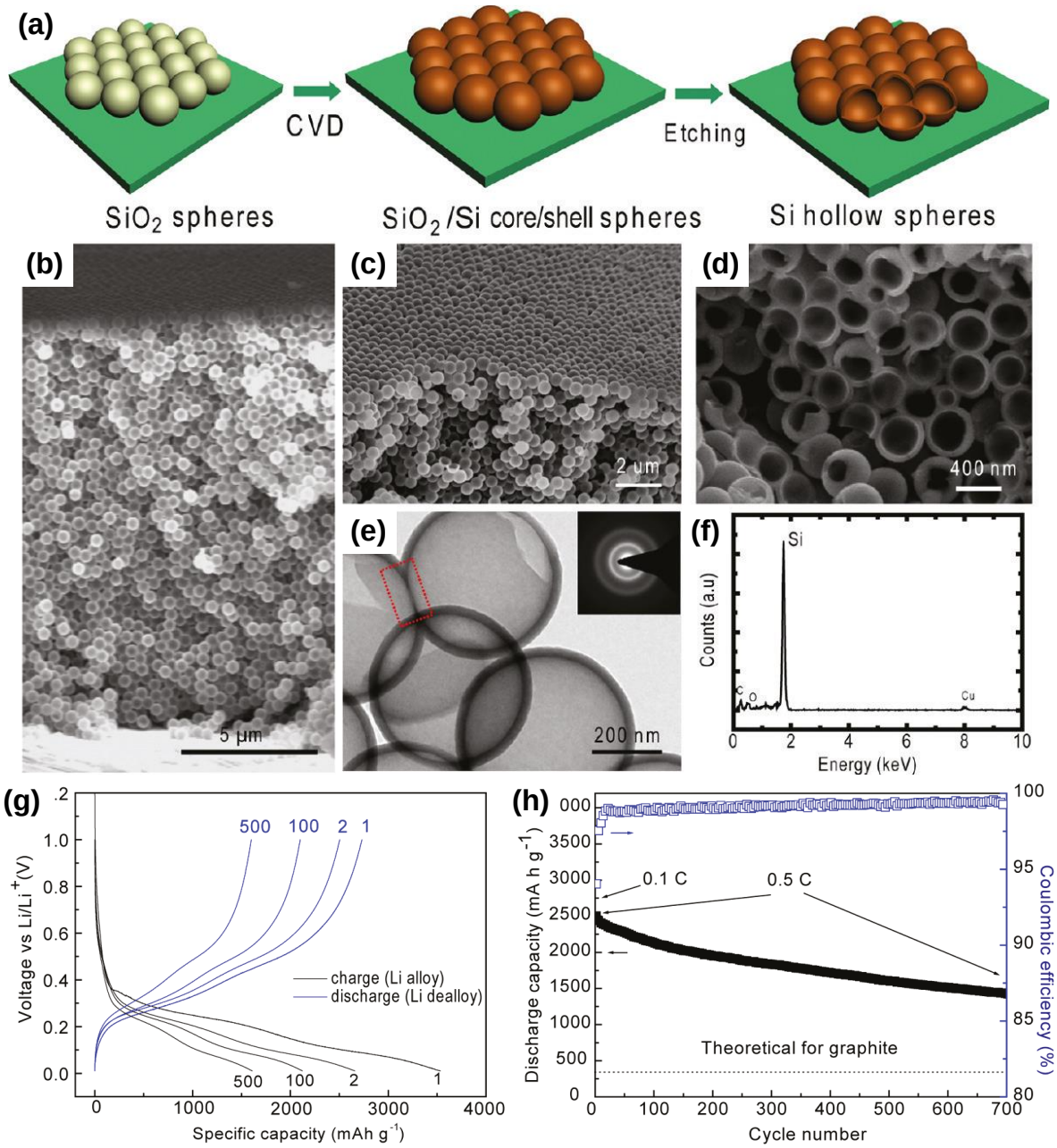

Figure 1.4. (a) Schematic illustration of hollow nanosphere synthesis, (b) cross-sectional and (c) side view SEM image of hollow Si spheres, (d) SEM image of scraped hollow Si spheres, (e) TEM image of interconnected hollow Si spheres, (f) energy dispersive X-ray spectroscopy (EDS) of hollow Si spheres, (g) charge/discharge profiles until 500th cycles, and (h) cycle performance and coulombic efficiency of hollow Si spheres.[30]

1.2.3 Separators

A separator is a permeable membrane placed between cathode and anode, which keeps the two electrodes physically apart.[37-38] In lithium-based cells, the essential functions of separator are the prevention of electronic contact while enabling ionic transport between positive and negative electrodes and a good shutdown properties, related to battery safety.[38] Generally, most separators consist of a polymeric membrane forming a microporous layer, and polymer is usually used polyolefin, polyethylene (PE) or polypropylene (PP).[5]

Separator can be classified into many types, including microporous, nonwoven, ion exchange membranes, supported liquid membranes, polymer electrolyte or solid ion conductors. Especially, polymer electrolyte and solid ion conductors that combine the separator and the electrolyte into a single component have been recently developed.[37]

The requirements of separators are stated as follows: (i) thickness, (ii) gurley (air permeability), (iii) porosity, (iv) wettability, and (v) chemical stability. First, the thickness of separator has to be less than 25 μm for portal electronic devices, but the thicker separator (40 μm) is needed to the EV/HEV applications.[39] And gurley value is proportional to electrical resistivity, for a given separator morphology. In LIBs, the gurley value of separator should be low (~25) because of good electrical performance.[37] Also, the porosity of separators have >40% and control of porosity is very important for the rate capability of LIBs.[40] The proper pore size is proper from 100 nm to 0.1 mm in order to prevent lithium dendrite penetration.[38, 40] Moreover, separator should be wet quickly and completely in typical electrolyte, and should be chemically stable. For example, polyolefin-based separator exhibit a high resistance to most of the conventional chemicals and good mechanical properties. A role of separator is very important at high temperature, related to the safety.[37,41] When the temperature become over 130 ^{o}C, the thermal shutdown of batteries exhibits a large increase in impedance that effectively stops ionic transport between the electrodes.[41,42]

Separator is not contribute the specific capacity of LIBs directly, but its structure and properties indirectly affect the electrochemical performances, including an energy and power densities, a cycle life, and a safety.

Table 1.3. General requirements for LIBs separator.[37]

Parameter	Requirements
Thickness (μm)	<25
Electrical resistance (MacMullin no., dimensionless)	<8
Gurley (s)	~25
Pore size (μm)	<1
Porosity (%)	~40
Tensile strength (%)	<2% offset at 1000 psi
Shutdown temperature (°C)	~130
High-temp melt integrity (°C)	>150
Wettability	Complete wet out in typical battery electrolytes
Chemical stability	Stable in battery for long period of time
Dimension stability	Separator should lay flat; be stable in electrolyte

1.2.4 Electrolytes

An electrolyte is a substance that dissociates in organic solvent to form ions, thus increasing the extent to which the liquid conducts electricity.[43] As a result, electrolyte transport ions from one electrode to another electrodes. When the charging, lithium ions were dissociated from the cathode and they were transported through the electrolyte. Finally, lithium ions reacted with the anode active material. The most common electrolyte is an ionic solution, but molten electrolytes and solid electrolytes are also possible.[7]

Typically, liquid electrolytes are composed of organic solvents, lithium salts, and additives. The most common organic solvents are mixture of the cyclic carbonate such as ethylene carbonate (EC) or propylene carbonate (PC), and linear carbonate such as dimethyl carbonate (DMC), diethyl carbonate (DEC), and ethyl methyl carbonate (EMC).[44] Their structure and characteristics are shown in Table 1.4.[43]

In case of the organic solvents, these should meet several requirements. First, the organic solvents should be inert to all of cell components, especially charged surfaces of cathode and anode.[43] Second, the organic solvents should have a high dissolution ability of lithium salt, in other words, it should have a high dielectric constant.[45] However, a high dielectric constant causes a high viscosity, and an ionic conductivity will be decreased. Third, the viscosity of organic solvents has to be low. Viscosity is the measure of a liquid resistance to flow. If the viscosity of solvent is high, ionic mobility will be decreased, leading to a low ionic conductivity. Therefore, the movement of lithium ions will be interrupted in LIBs.[46] Fourth, a wide temperature range has to be required, means that a melting point is as low as possible and a boiling point is as high as possible.[47] Because low melting point of electrolyte guarantees the ion conduction at low temperature, and thus a LIBs can be used to get the electric energy. Fifth, the electrolyte should be safe, nontoxic, and economical. Most of organic solvents are flammable at the elevated temperature, so, the flash point of electrolytes has to be high.[48] It is difficult to meet all those requirements because of complicated considerations. Therefore, many researches have been developed to find advanced electrolytes for the next generation LIBs.

Table 1.4. Representative cyclic and linear carbonates as electrolyte solvents and their characteristics.[43]

Solvent	Structure	Molecular weight	T_m (°C)	T_b (°C)	T_f (°C)	ε (25 °C)	η/cP (25 °C)
EC	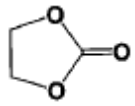	88	36.4	248	160	89.78	1.90 (40 °C)
PC	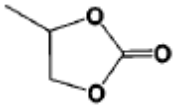	102	-48.8	242	132	64.92	2.53
DMC	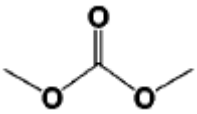	90	4.6	91	18	3.107	0.59
DEC	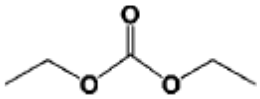	118	-74.3	126	31	2.805	0.75
EMC	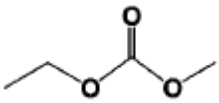	104	-53	110		2.958	0.65

1.3 References

1. Choi, N.-S.; Chen, Z.; Freunberger, S. A.; Ji, X.; Sun, Y.-K.; Amine, K.; Yushin, G.; Nazar, L. F.; Cho, J.; Bruce, P. G., Challenges Facing Lithium Batteries and Electrical Double-Layer Capacitors. *Angewandte Chemie International Edition* **2012**, 51 (40), 9994-10024.
2. Palomares, V.; Serras, P.; Villaluenga, I.; Hueso, K. B.; Carretero-González, J.; Rojo, T., Na-ion batteries, recent advances and present challenges to become low cost energy storage systems. *Energy & Environmental Science* **2012**, 5, 5884.
3. Winter M.; Brodd R. J., What Are Batteries, Fuel Cells, and Supercapacitors? *Chemical Reviews* **2004**, 104, 4245-4269
4. Jeong, G.; Kim, Y.-U.; Kim, H.; Kim, Y.-J.; Sohn, H.-J., Prospective materials and applications for Li secondary batteries. *Energy & Environmental Science* **2011**, 4, 1986
5. Dunn, B.; Kamath, H.; Tarascon, J. M., Electrical Energy Storage for the Grid: A Battery of Choices. *Science*, **2011**, 334, 928-935
6. Bruce, P. G.; Scrosati, B.; Tarascon, J.-M., Nanomaterials for Rechargeable Lithium Batteries. *Angewandte Chemie International Edition* **2008**, 47, 2930-2946.
7. Park, J.-K., *Principles and Applications of Lithium Secondary Batteries*. Wiley-VCH Verlag GmbH & Co. KGaA : 2012.
8. Tarascon, J.-M.; Armand, M., Issues and challenges facing rechargeable lithium batteries. *Nature* **2001**, 414 (6861), 359-367.
9. Manz AG Home Page. http://www.manz.com/growth-markets/battery (accessed Dec 3, 2014).
10. Song, M.-K.; Park, S.; Alamgir, F. M., Cho, J., Liu, M., Nanostructured electrodes for lithium-ion and lithium-air batteries: the latest developments, challenges, and perspectives. *Materials Science and Engineering: R* **2011**, 72, 203-252.
11. Zhou, G.; Li, F.; Cheng, H.-M., Progress in flexible lithium batteries and future prospects. *Energy & Environmental Science* **2014**, 7, 1307.
12. Song, H. -K.; Lee, K. T.; Kim, M. G.; Nazr, L. F.; Cho, J., Recent Progress in Nanostructured Cathode Materials for Lithium Secondary Batteries. *Advanced Functional Materials* **2010**, 20, 3818-3834.
13. Takahashi, Y.; Tode, S.; Kinoshita, A.; Fujimoto, H.; Nakane, I.; Fujitani, S, Development of Lithium-Ion Batteries with a $LiCoO_2$ Cathode Toward High Capacity by Elevating Charging Potential. *Journal of The Electrochemical Society* **2008**, 155 (7), A537-A541.
14. Cho, J.; Kim, C.-S.; Yoo, S.-I., Improvement of Structural Stability of $LiCoO_2$ Cathode during Electrochemical Cycling by Sol-Gel Coating of SnO_2. *Electrochemical and Solid-State Letters* **2000**, 3 (8), 362-365.

15. Lee, J.-I.; Lee, E.-H., Park, J.-H.; Park, S.; Lee, S.-Y., Ultrahigh-Energy-Density Lithium-Ion Batteries Based on a High-Capacity Anode and a High-Voltage Cathode with an Electroconductive Nanoparticle Shell. *Advanced Energy Materials* **2014**, 4(8), 1301542-1301550.
16. Islam, M. S.; Fisher, C. A., Lithium and sodium battery cathode materials: computational insights into voltage, diffusion and nanostructural properties. Chem Soc Rev, 2014, 43, 185-204.
17. Arai, H.; Okada, S.; Sakurai, Y.; Yamaki, J.-i., Reversibility of $LiNiO_2$ cathode. *Solid State Ionics* **1997**, 95, 275-282.
18. Etacheri, V.; Marom, R.; Elazari, R.; Salitra, G.; Aurbach, D., Challenges in the development of advanced Li-ion batteries: a review. *Energy & Environmental Science*, **2011**, 4 (9), 3243-3262
19. OHZUKU, T.; UEDA, A.; NAGAYAMA, M.; IWAKOSHI, Y.; KOMORI, H., COMPARATIVE STUDY OF $LiCoO_2$, $LiNi_{1/2}Co_{1/2}O_2$ AND $LiNiO_2$ FOR 4 VOLT SECONDARY LITHIUM CELLS. *Electrochemica Acta* **1993**, 38(9), 1159-1167.
20. Zhang, Q.; Uchaker, E.; Candelaria, S. L.; Cao, G., Nanomaterials for energy conversion and storage. *Chemical Society Reviews* **2013**, 42, 3127-3171.
21. Jang, D. H.; Oh, S. M., Electrolyte Effects on Spinel Dissolution and Cathodic Capacity Losses in 4 V $Li/Li_xMn_2O_4$ Rechargeable Cells. *Journal of The Electrochemical Society* **1997**, 144 (10), 3342-3348.
22. Tarascon, J.; Wang, E.; Shokoohi, F.; McKinnon, W.; Colson, S., The Spinel Phase of $LiMn_2O_4$ as a Cathode in Secondary Lithium Cells. *Journal of The Electrochemical Society* **1991**, 138 (10), 2859-2864.
23. Manthiram, A.; Murugan, A. V.; Sarkar, A.; Muraliganth, T., Nanostructured electrode materials for electrochemical energy storage and conversion. Energy Environmental Science 2008, 1, 621-638.
24. Mladenov, M.; Stoyanova, R.; Zhecheva, E.; Vassilev, S., Effect of Mg doping and MgO-surface modification on the cycling stability of $LiCoO_2$ electrodes. *Electrochemistry Communications* **2001**, 3, 410-416.
25. Yoshio, M.; Wang, H.; Fukuda, K.; Hara, Y.; Adachic, Y., Effect of Carbon Coating on Electrochemical Performance of Treated Natural Graphite as Lithium-Ion Battery Anode Material. *Journal of The Electrochemical Society* **2000**, 147 (4), 1245-1250.
26. Huggins, R. A., Lithium alloy negative electrodes. *Journal of Power Sources* **1999**, 81-82, 13-19.
27. Hatchard, T. D.; Dahn J. R., In Situ XRD and Electrochemical Study of the Reaction of Lithium with Amorphous Silicon. *Journal of The Electrochemical Society* **2004**, 151 (6), A838-A842.

28. Kasavajjula, U.; Wang, C.; Appleby, A. J., Nano- and bulk-silicon-based insertion anodes for lithium-ion secondary cells. *Journal of Power Sources* **2007**, 163, 1003-1039.
29. CHAN, C. K.; PENG, H.; LIU, G.; McILWRATH, K.; ZHANG, X. F.; HUGGINS, R. A.; CUI, Y., High-performance lithium battery anodes using silicon nanowires. *Nature* **2008**, 3, 31-35.
30. Yao, Y.; McDowell, M. T.; Ryu, I.; Wu, H.; Liu, N.; Hu, L.; Nix, W. D.; Cui, Y., Interconnected Silicon Hollow Nanospheres for Lithium-Ion Battery Anodes with Long Cycle Life. *Nano Letters* **2011**, 11, 2949–2954.
31. Park, O.; Lee, J.-I.; Chun, M.-J.; Yeon, J.-T.; Yoo, S.; Choi, S.; Choi, N.-S.; Park, S., High-performance Si anodes with a highly conductive and thermally stable titanium silicide coating layer. *RSC Advances* **2013**, 3, 2538-2542.
32. Xiang, H.; Zhang, K.; Ji, G.; Lee, J. Y.; Zou, C.; Chen, X.; Wu, J., Graphene/nanosized silicon composites for lithium battery anodes with improved cycling stability. *CARBON* **2011**, 49, 1787-1796.
33. Park, M. S.; Ma, S. B.; Lee, D. J.; Im, D.; Doo, S.-G.; Yamamoto, O., A Highly Reversible Lithium Metal Anode. *SCIENTIFIC REPORTS* **2014**, 4 (3815), 1-8.
34. Wang, L.; Wang, D.; Dong, Z.; Zhang, F.; Jin J., Interface Chemistry Engineering for Stable Cycling of Reduced GO/SnO2 Nanocomposites for Lithium Ion Battery. *Nano Letters* **2013**, 13, 1711−1716.
35. Deng, D.; Lee, J. Y., Reversible Storage of Lithium in a Rambutan-Like Tin–Carbon Electrode. *Angewandte Chemie International Edition* **2009**, 48, 1660-1663.
36. Zhang, W.-J., A review of the electrochemical performance of alloy anodes for lithium-ion batteries. *Journal of Power Sources* **2011**, 196, 13-24.
37. Arora, P.; Zhang Z., Battery Separators. *Chemical Reviews* **2004**, 104, 4419-4462.
38. Lee, H.; Yanilmaz, M.; Toprakci, O.; Fu, K.; Zhang, X., A review of recent developments in membrane separators for rechargeable lithium-ion batteries, *Energy & Environmental Science* **2014**, 7, 3857-3886.
39. Palacín, M. R., Recent advances in rechargeable battery materials: a chemist's perspective. *Chemical Society Reviews* **2009**, 38, 2565–2575.
40. Orendorff, C. J., The Role of Separators in Lithium-Ion Cell Safety. *The Electrochemical Society Interface* **Summer 2012**, 61-65.
41. Zhang, S. S., A review on the separators of liquid electrolyte Li-ion batteries. *Journal of Power Sources* **2007**, 164, 351–364.
42. Chung, Y. S.; Yoo, S. H.; Kim, C. K., Enhancement of Meltdown Temperature of the Polyethylene Lithium-Ion Battery Separator via Surface Coating with Polymers Having High Thermal Resistance. *Industrial & Engineering Chemistry Research* **2009**, 48, 4346–4351.

43. Xu, K., Nonaqueous Liquid Electrolytes for Lithium-Based Rechargeable Batteries. *Chemical Reviews* **2004**, 104, 4303-4417.
44. Yamada, Y.; Sagane, F.; Iriyama, Y.; Abe, T.; Ogumi, Z., Kinetics of Lithium-Ion Transfer at the Interface between $Li_{0.35}La_{0.55}TiO_3$ and Binary Electrolytes. *The Journal of Physical Chemistry C* **2009**, 113, 14528–14532.
45. Jouyban, A.; Soltanpour, S.; Chan, H.-K., A simple relationship between dielectric constant of mixed solvents with solvent composition and temperature. *International Journal of Pharmaceutics* **2004**, 269, 353-360.
46. Gering, K. L., Prediction of electrolyte viscosity for aqueous and non-aqueous systems: Results from a molecular model based on ion solvation and a chemical physics framework. *Electrochimica Acta* **2006**, 51, 3125-3138.
47. Zhang, S. S.; Xu K.; Jow, T. R., An improved electrolyte for the LiFePO4 cathode working in a wide temperature range. *Journal of Power Sources* **2006**, 159, 702–707.
48. Xu, K.; Zhang, S.; Allen, J. L.; Jow, T. R., Nonflammable Electrolytes for Li-Ion Batteries Based on a Fluorinated Phosphate. *Journal of The Electrochemical Society* **2002**, 149 (8), A1079-A1082.

II. Synthesis of highly dispersive and electrically conductive silver-coated silicon of anode material for lithium ion batteries

2.1 Introduction

In the past decades, there has been great interest in developing advanced electrode materials for lithium-ion batteries (LIBs) with high power and energy densities that meet the requirements for hybrid electric vehicles (HEVs) and electric vehicle (EVs) applications.[1-4] Lithium alloying compounds (e.g., Si, Ge, Al, Sn, Sb, etc.) have been intensively studied, since such electrodes provide much higher theoretical specific capacity than that of graphite anodes (~372 mAh g^{-1}) used in conventional LIBs.[5-7] Among them, Si has been considered the most promising anode materials due to its high theoretical specific capacity (>3500 mAh g^{-1} at room temperature), low lithiation potential (<0.5 V vs. Li/Li^+), low cost, and environmental safety.[8-14] The commercial use of Si powder is, however, still hindered owing to two major problems. One is the low intrinsic electrical conductivity of Si and the other is a large volume change (>300%) during the alloying/de-alloying reaction of Si with Li^+ ions ($Si + xLi^+ + xe^- \leftrightarrow Li_xSi$ ($0 \leq x \leq 4.4$), which leads to pulverization and causes significant capacity loss.[8-10]

The use of nanostructured materials (e.g., nanoparticles, nanowires, nanotubes, hollow structures) is a typical approach for improving the electrochemical properties of these electrodes.[11-16] Compared to bulk materials, nanomaterials have several advantages, including (i) a higher interfacial area that can enhance charge/discharge rates, (ii) shorter path lengths of Li^+ ion transport that increase power capabilities, and (iii) release of the mechanical strain during lithiation/delithation process that can improve the cycling life. However, the nanostructured electrodes also have several disadvantages, including (i) a serious side reaction due to a high surface activity, (ii) a low tap density related to the large surface-to-volume ratio, and (iii) a tendency of aggregation during the lithiation/delithiation process that degrades the cycling life.

To emphasize the advantages and minimize the disadvantages of Si-based nanomaterials, a rich variety of methods have been developed, such as dispersing Si into an inactive/active matrix,[17,18] design of novel structures,[19-22] surface coating with an inactive layer,[23,24] and surface coating with electronically conductive layer.[25-27] Among them, a simple, but straightforward route is to coat the Si surface with conductive materials which can enhance the electrical conductivity of Si and may alleviate a large volume change during cycling. Typically, carbon coating process has been used with several advantages, like (i) preventing aggregation of Si particles, (ii) buffering a large volume change, (iii) forming a stable solid-electrolyte interface (SEI) layer, and (iv) increasing the electrical conductivity.[10,14,19,20] However, the carbon coating process requires high-temperature process (>700 °C), such as a carbonization of carbon source materials or thermal decomposition of acetylene gas.

To further enhance electrical conductivity of Si-based materials, metal coating process (e.g., Ag, Fe, Co, and Cu) is one of the effective methods which can be used at relatively low temperature.[28-32] For example, Yu et al. reported that Ag nanoparticles were coated on the surface of Si particles via Ag-mirror reaction process, resulting in improving the battery performance and reversible lithium storage capacity.[32] As another example, Cu deposition on the Si surface enhanced the electrical conductivity of Si particles, leading to increasing initial coulombic efficiency and capacity retention, compared to carbon-coated Si electrodes.[28,30,33] Above mentioned examples have been used a multi-step process to coat the metal particles on the Si surface.

Herein, we report a simple chemical approach for synthesizing Ag-coated Si nanoparticles via a one-pot reduction process in the presence of alkylamine at low temperature, in which Ag-amine complex suppresses the growth of Ag nanoparticles, leading to a uniform Ag coating on a Si surface. The Ag-coated Si particles are highly dispersive in aqueous and alcoholic solvents and significantly increase the electrical conductivity of Si electrodes. These results demonstrate that highly conductive Ag-coated Si electrodes (i) reduce charge transfer resistance, (ii) increase a specific reversible capacity, (iii) enhance a cycling stability, (iv) improve a high rate capability, and (v) alleviate a large volume change during cycling.

2.2 Experimental

2.2.1 Synthesis of silver-coated silicon

To synthesize the silver-coated silicon, 0.25 g of Si powder with average diameter of 50nm (Aldrich) was dispersed into 20 mL of ethanol at 50 ºC in a propylene reactor. The propylene reactor avoids any binding between Ag ions and the container. And then, 5-200 mM of silver nitrate ($AgNO_3$, Aldrich) was added to the solution and 1.5-200 mM of n-butylamine (Aldrich) was added subsequently. To know the variation of silver coverage on the silicon surface, the molar ratio of $AgNO_3$/butylamine and the $AgNO_3$ concentration were controlled. After stirring for 10 min, Ag-coated Si particles were rinsed with ethanol to remove residual Ag precursors. Finally, it was filtered out and dried at 80 ºC for 12 h in a vacuum oven.

2.2.2 Characterization of silver-coated silicon

The morphology of bare Si and Ag-coated Si were characterized by a transmission electron microscopy (TEM, JEM-1400) operating at the acceleration voltage of 120 kV. For the TEM measurement, the silver-coated silicon was dispersed in the ethanol, and then transferred on the Formvar-coated coppoer grid. The high power X-ray diffractometer (Rigaku D/MAX) at 2500 V was performed in order to investigate the microstructures of bare Si and Ag-coated Si particles. To compare the dispersion of bare Si and Ag-coated Si, both samples were measured by a scanning electron microscope (SEM, Nano SEM 230, FEI) operating at 10 kV. The electrical conductivities of bare Si and Ag-coated Si were measured thorough a four point probe method using Advanced Instrument Technology (AIT) CMT-SR1000N.

2.2.3 Electrochemical tests

The electrochemical properties of bare Si and Ag-coated Si electrodes were tested by galvanostatic discharging and charging in coin-type half cells (2016 R-type). The cells that were composed of active material/super P carbon black/binder composite as a working electrode and lithium metal as a counter electrode, were prepared in an argon-filled glove box. The electrode was composed of active material (bare Si or Si@Ag, 70 wt%), super P carbon black (10 wt%), and poly(acrylic acid)/sodium carboxymethyl cellulose (50/50 wt%/wt%, Aldrich) binder (20 wt%). The resulting slurry was coated on a Cu current collector and dried in a vacuum oven at 150 ºC for 2h. The electrolyte was composed of 1.3M $LiPF_6$ in ethylene carbonate/diethyl carbonate (EC/DEC, 30/70 v/v, Panaxetec) with 10 wt% fluoroethylene carbonate (FEC). The cells were cycled at a rate of 0.05-20 C between 0.005-1.5 V (vs. Li/Li^+). All electrochemical measurements were carried out with a WBCS-3000 battery cycler (Wonatech Co.) at room temperature.

2.3 Results and discussion

Typically, silver coated silicon particles have been synthesized through a silver-mirror reaction that silver nitrate ($AgNO_3$) was directly reduced by a glucose, the average Ag particle size of <200 nm.[31,32,34] In this study, we used a butylamine as a reducing agent instead of glucose, so, 0.25 g of Si powder was dispersed into 20 mL of ethanol at 50 °C, and then, 5 mM of $AgNO_3$ was added to the solution and 5 mM of butylamine was added subsequently with 10 min stirring. In general, the solubility of $AgNO_3$ in alcohol solvent is a quite low, however, when amine-based chemical is added, the solubility of Ag precursors in ethanol enhances significantly.[31,32,34] Compared to a strong reducing agent (e.g., $NaBH_4$, NH_2NH_2), the butylamine slowly reduces Ag precursors to Ag nanoparticle. In the presence of alkylamine, Ag nanoparticles are grew by the following complex equilibrium.[34]

$$[Ag(R\text{-}NH_2)_2]^+ \leftrightarrow [Ag(R\text{-}NH_2)]^+ + R\text{-}NH_2 \quad (1)$$

$$[Ag(R\text{-}NH_2)]^+ \leftrightarrow Ag^+ + R\text{-}NH_2 \quad (2)$$

The Ag-amine complex ions gradually release Ag^+ ions for a slow reduction process and Ag nanoparticles are formed with the size of <20 nm on the Si surface (Scheme in Figure 2.1). The size of Ag particles and the surface coverage can be tuned easily by controlling the ratio of butylamine and $AgNO_3$, consequently the dimension of Ag nanoparticles can be changed.

Figure 2.1 shows TEM images of Ag-coated Si nanoparticles synthesized via a chemical reduction of Ag precursor in the presence of butylamine. As-synthesized Ag-coated Si particles were deposited on a Formvar-coated copper grid to characterize the size of Ag particles. The Ag nanoparticles were uniformly coated on the Si surface with an average diameter of 13 nm (Figure 2.1.a & 2.1.b). It should be noted that the as-synthesized Ag-coated Si nanoparticles are suspended well in water and ethanol, while bare Si particles are aggregated in the bottom of solution. In order to investigate the dispersion of bare Si and Ag-coated Si particles in H_2O, 10 mg of Si (or Ag-coated Si) was dispersed in 3 mL of H_2O and drop casted on Si substrates. The Ag-coated Si particles were highly dispersed without any aggregation, while the bare Si particles were aggregated seriously each other (Figure 2.1c & 2.1d). The magnified SEM images showed more clearly the dispersion of both samples (Figure 2.2).

Figure 2.1.e shows the X-ray diffraction (XRD) patterns of bare Si and Ag-coated Si particles. The bare Si showed a pure crystalline Si and a small amount of native oxide (SiO_x). However, Ag-coated Si showed three additional diffraction peaks at $2\theta = 38.2^o$, 44.4^o, 64.6^o that correspond to (111), (200), and (220) planes of face-centered cubic Ag (JCPDS Card No. 4-783). From the XRD patterns, we calculated the crystal size (~7.8 nm) of the Ag using the Scherrer equation, $L = 0.9\lambda/(B\cdot\cos\theta)$, where L is the diameter of the crystallites, λ is the X-ray wavelength, B is the full width at half maximum, and θ is the Bragg angle.[35] The result is similar as an average particle size (~7 nm) obtained from TEM. Morever, the Ag content was measured as ~3 wt% by inductively coupled plasma mass spectrometry (ICP-MS).

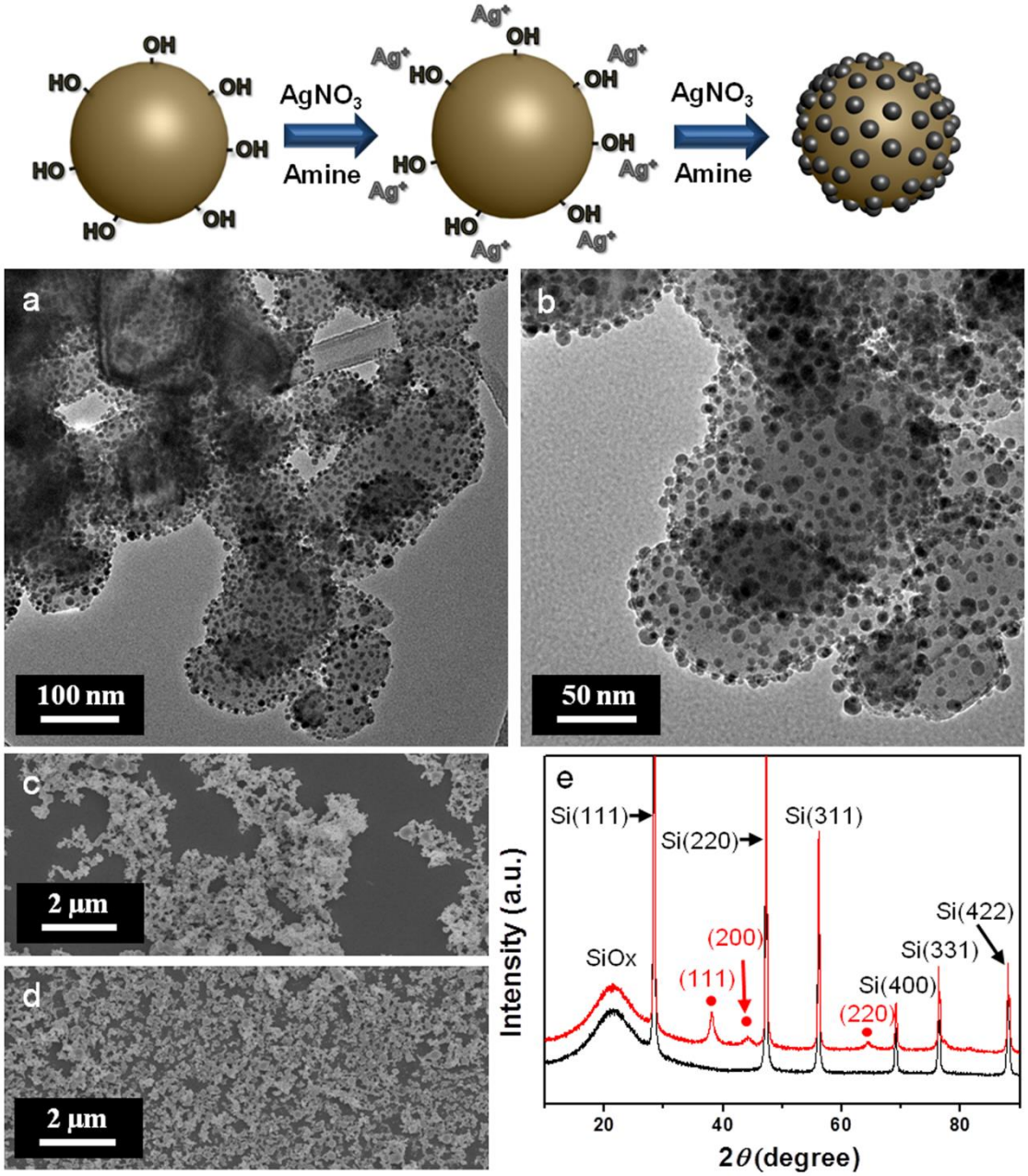

Figure 2.1. Top: schematic illustration showing synthetic route of Ag-coated Si. Bottom: (a), (b) TEM images of Ag-coated Si synthesized by a chemical reduction of 5 mM $AgNO_3$ with 5 mM butylamine. SEM images of (c) bare Si and (d) Ag-coated Si prepared on Si substrates. (e) XRD patterns of bare Si (black) and Ag-coated Si (red)

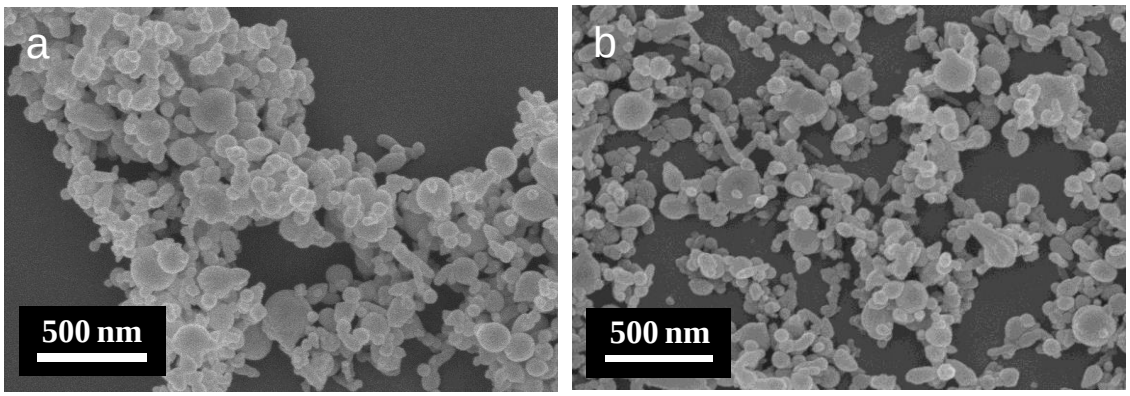

Figure 2.2. SEM images of (a) bare Si and (b) Ag-coated Si particles dispersed on the Si substrates.

The particle size and surface coverage of Ag nanoparticles on the Si surface can be controlled by various molar ratio of $AgNO_3$/butylamine as shown in Figure 2.3. When a fixed concentration of 5mM $AgNO_3$ reacts with 1.5, 5, 10, and 20 mM of butylamine in ethanol solution containing 0.25 g Si powders, Ag nanoparticles with an average particle size of 4, 7, 14, and 15 nm were decorated on the Si surfaces, respectively. When a small molar ratio of butylamine/$AgNO_3$ (0.3) was used, small Ag nanoparticles of ~4 nm were formed due to insufficient reduction reaction (Figure 2.3.a). With increasing the molar ratio of butylamine/$AgNO_3$, Ag particle size was also increased and reached plateau at molar ratio of ~4 (Inset of Figure 2.3.a). Considering Ag particle size and surface coverage, the equal amounts of $AgNO_3$ and butylamine are best condition to make Ag-coated Si nanoparticles (Figure 2.3.b). It should be noted that there is no any colloidal Ag particles formed in the solution, it means that no nucleation center existed in the solution, because butylamine is a very weak reducing agent.[36,37]

Moreover, we investigated the effect of the amount of $AgNO_3$ and butylamine with a fixed molar ratio ($AgNO_3$/butylamine = 1) on the size and surface coverage of Ag nanoparticles. When the concentration of $AgNO_3$ was tuned from 10 to 200 mM, an average diameter of Ag nanoparticles steadily increased, but Ag nanoparticles were seriously aggregated with a high surface coverage (Figure 2.4). From a plot of Ag content versus concentration of $AgNO_3$, we can see that surface coverage of Ag nanoparticles is exponentially increased at low $AgNO_3$ concentration regions (5-50 mM), and steadily increased at high concentration (100-200 mM) (Figure 2.5).

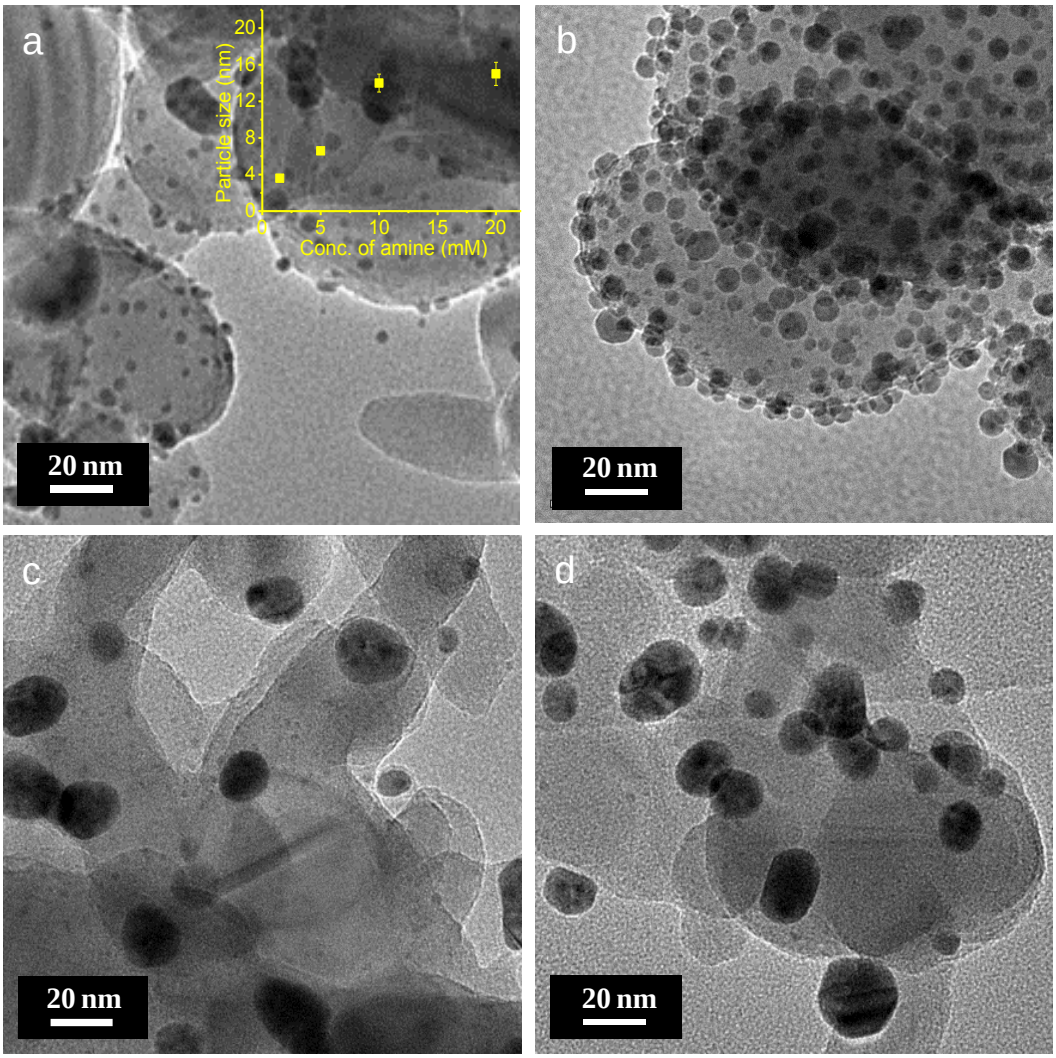

Figure 2.3. TEM images of Ag-coated Si synthesized by four different molar ratios of $AgNO_3$ and butylamine. 5mM of $AgNO_3$ reacts with (a) 1.5mM, (b) 5mM, (c) 10mM, and (d) 20mM of butylamine at 50 ^oC for 10 min. Inset of Figure 2(a) shows the average Ag particle size as a function of butylamine concentration.

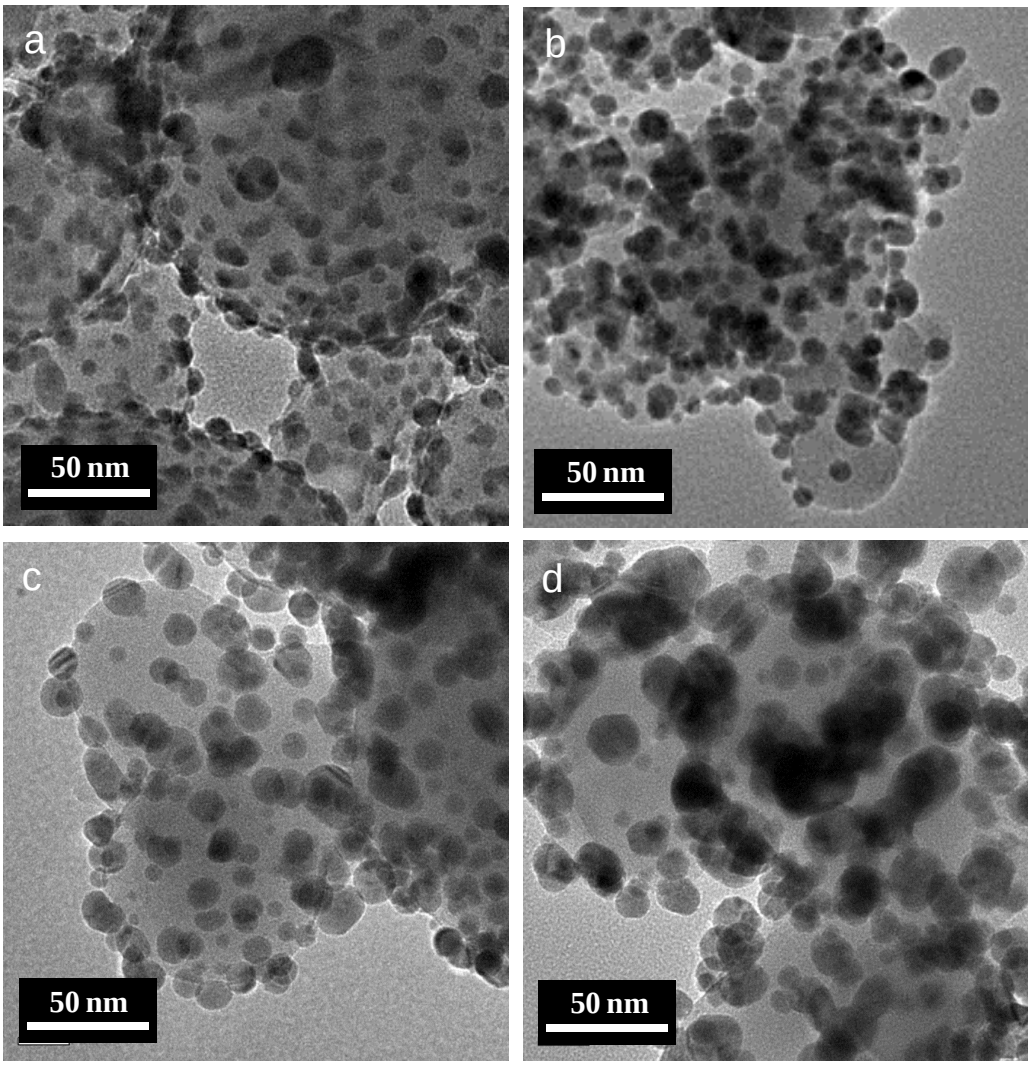

Figure 2.4. TEM images of Ag-coated Si synthesized by a fixed molar ratio ($AgNO_3$/butylamine = 1) but four different concentrations of (a) 10 mM, (b) 50 mM, (c) 100 mM, and (d) 200 mM of $AgNO_3$ and butylamine.

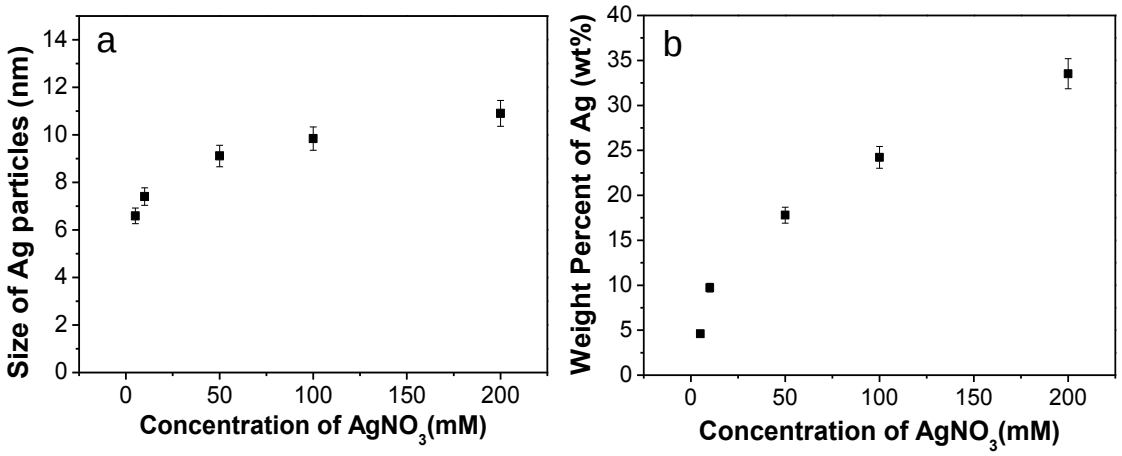

Figure 2.5. Ag particle size and weight percent of Ag as a function of $AgNO_3$ concentration. (a) Particle size versus concentration of $AgNO_3$ and (b) Ag contents versus concentration of $AgNO_3$. Ag-coated Si particles were prepared by several different $AgNO_3$ concentrations with a fixed molar ratio ($AgNO_3$/butylamine = 1).

The electrochemical performances of bare Si and Ag-coated Si particles as anodes in LIBs was tested with a coin-type half (2016R) within 0.005-1.2 V (vs. Li/Li^+). In case of the Ag-coated Si electrode, sample that contained 3 wt% of Ag content was used to minimize an alloying reaction between lithium and Ag, since Ag particles can alloy with lithium below 0.1 V.[38]

Figure 2.6.a shows the first cycle discharge (lithiation) and charge (delithiation) voltage profiles of the bare Si and the Ag-coated Si electrodes at 0.1 C rate. The bare Si shows first discharge capacity of 1690 mA h g^{-1} and charge capacity of 1300 mA h g^{-1}, respectively, corresponding to a coulombic efficiency of 76.9%. The specific charge capacity of the bare Si electrode was significantly decreased due to the poor electrical conductivity of Si materials. However, the Ag-coated Si electrode exhibited a discharge capacity of 1940 mA h g^{-1} and a charge capacity of 1550 mA h g^{-1}, indicating an enhanced coulombic efficiency of 80%. The increased charge capacity of the Ag-coated Si is attributed to the enhnacement of electrical conductivity. When the conductivity of both electrodes were measured by four point probe method, the electrical conductivity of the Ag-coated Si (1.62×10^{-4} S/cm) was one order of magnitude higher than that of the bare Si electrodes (3.07×10^{-5} S/cm). It should be noted that the Ag coating layer acted as the effective pathway for electrical conduction (Figure 2.8).

Figure 2.6.b shows differential capacity (dQ/dV vs. capacity) profiles of Ag-coated Si electrodes in the first (black) and second (red) cycles. In the first discharge (lithiation), one broad peak between 0.17-0 V is observed, which is attributed to the phase transition of amorphous Li_xSi phases to crystalline $Li_{15}Si_4$.[8, 39] And two broad peaks were observed at 0.28 V and 0.44 V during first charge (delithiation), which is due to the phase transition between amorphous Li_xSi and amorphous Si. Upon the second discharge, additional broad peak between 0.35 and 0.15 V was observed, resulting from overlapping of at least two reaction processes based on the two peaks appearing in the charging process.[39] The dQ/dV curves of Ag-coated Si is consistent with the previous results reported in the literature for Si electrode.[6,8,14,39,40] In typical, Ag particles can react with lithium to form lithium alloying.[38] However, any additional redox peaks were not observed until second cycles, indicating that small amounts of Ag nanoparticles (3 wt%) in the Ag-coated Si powder serve as a conducting additive. Meanwhile, the differential capacity profiles of bare Si electrode showed similar peak features below 0.3 V (versus Li/Li^+) compared to Ag-coated Si electrode, except for the shift of first cathodic peak from 0.08 V (bare Si) to 0.05 V (Ag-coated Si) because of the formation of different SEI layers (Figure 2.7).[39]

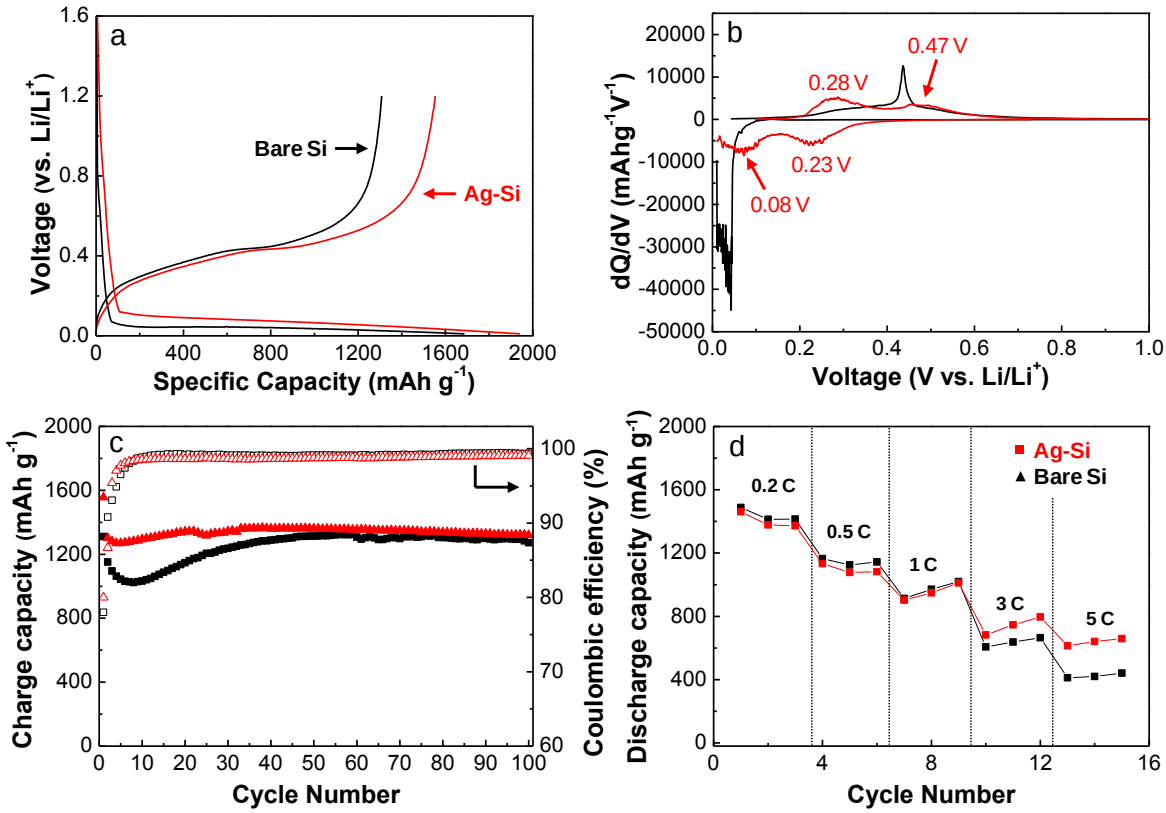

Figure 2.6. Electrochemical performances of bare Si and Ag-coated Si electrodes: (a) First cycle of bare Si and Ag-coated Si at 0.1 C in the range of 0.005-1.6 V, (b) differential capacity (d*Q*/dV) plots of both electrodes in the first and second cycles, (c) cycling performance and (d) rate capabilities (0.2-5 C) of bare Si and Ag-coated Si.

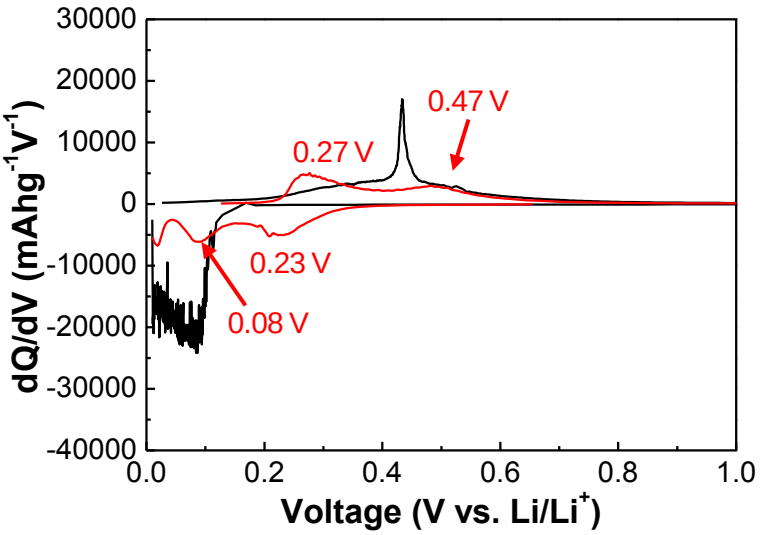

Figure 2.7. Differential capacity (dQ/dV) plots of bare Si electrode in the first (black) and second (red) cycles.

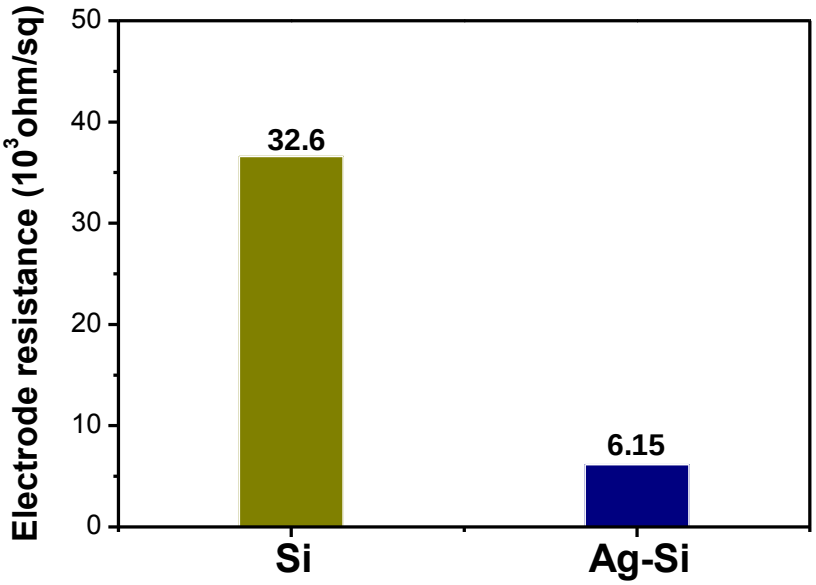

Figure 2.8. Electrical conductivities of bare Si and Ag-coated Si electrodes.

The charge capacity of Ag-coated Si electrode after 100 cycles was 1320 mAh g^{-1} at a 0.2 C rate, indicating the capacity retention of nearly 100%, compared to the second cycle charge capacity (Figure 2.6.c). However, the bare Si electrode showed a serious capacity fading until 30 cycles at the rate of 0.2 C, which is attributed to the internal resistance due to the formation of unstable SEI layers. The excellent cycling performance of Ag-coated Si electrode can be explained as follows: (i) electrically conductive Ag layers enhance the electrical conductivity of Si significantly. (ii) Nano-sized Si particles can withstand effectively the stress caused by the large volume change without fracture.[41] (iii) Ag-coating layers prevent the aggregation of Si nanopowders. And (iv) Ag-coating layers are mechanically strong, these can effectively prevent the pulverization of Si and support a stable SEI layer formation. These characteristics enabled the Ag-coated Si electrode to serve a fast discharging/charging process in LIBs. The rate capabilities in the range of 0.2 to 5 C rates of bare Si and Ag-coated Si electrode were plotted in figure 2.6.d. The bare Si electrode showed a reversible charge capacity of 420 mAh g^{-1} at 5 C rate, corresponding to the capacity retention of 29.8% compared to 0.2 C rate. In contrast, the Ag-coated Si exhibited an enhanced reversible capacity retention of 46.4% at 5 C rate, compared to the bare Si.

Additionally, excellent electrochemical performances of the Ag-coated Si electrode are attributed to stable Ag-coating and SEI layers. As mentioned before, the formation of stable SEI layers is one of the critical factors to obtain a stable cycling performance. When the potential where Si react with lithium was considered, the electrolyte used in this study will be decomposed inevitably on the Si surface. Therefore, continuous discharging and charging cycles cause the formation of thicker and thicker SEI layers on the Si surface. The electrically insulating SEI layers and the increase of lithium diffusion distance result in a low rate capability and a capacity fading.[22]

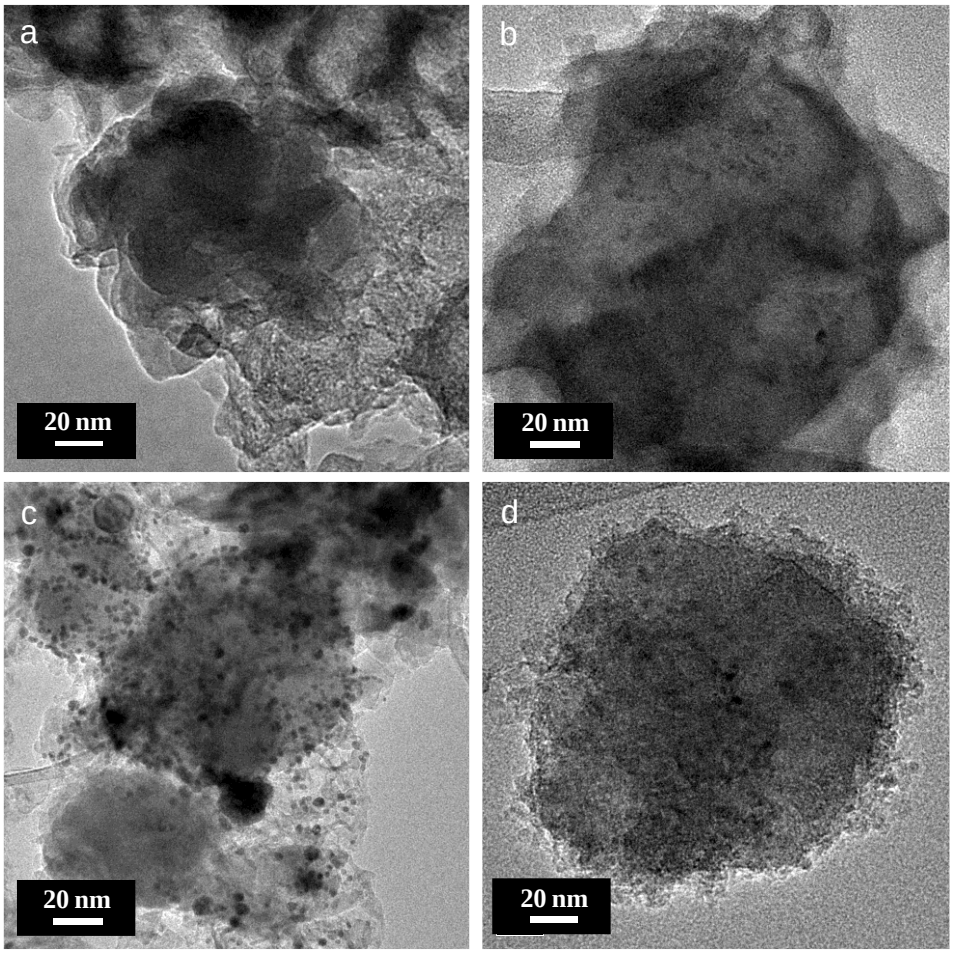

Figure 2.9. TEM images of bare Si ((a) and (b)) and Ag-coated Si ((c) and (d)) electrodes after 100 cycles.

In order to investigate morphologies and SEI layers of Si nanoparticles after cycling, we disassembled both electrodes and washed them with dimethyl carbonate (DMC) to remove a residual $LiPF_6$-based electrolyte. Figure 2.9 shows TEM images of the bare Si and the Ag-coated Si electrodes after 100 cycles. The morphology of bare Si particles changed from spherical shape to sponge-like structures and serious aggregations of Si nanoparticles were observed due to a formation of thick SEI layers and a large volume change on repeated cycling (Figure 2.9.a & 2.9.b). In contrast, the morphology of Ag-coated Si particles was similar to that of as-synthesized Ag-coated Si, except for the thin SEI formation (Figure 2.9.c & 2.9.d). It should be noted that the Ag-coated Si nanoparticles maintain structurally intact and Ag nanoparticles are still attached to the Si surface even after 100 cycles, providing the excellent electrochemical performance. Moreover, Ag nanoparticles greatly reduce the aggregation of Si nanoparticles, giving a stable cycling performance of active materials.

The electrochemical impedance spectra (EIS) of bare Si and Ag-coated Si electrodes were also measured to investigate the effect of Ag coating layer on the cycling performance. The AC impedance spectra of cells after 100 cycles were analyzed (Figure 2.10). A semicircle at the high frequency region indicates the diffusion resistance of Li ions through the SEI layer (R_{SEI}). The cell impedance of the bare Si electrode was R_{SEI} = 167 Ω, while the Ag-coated Si exhibited a significantly reduced diffusion resistance, R_{SEI} = 100 Ω. It may be attributed to the uniform dispersion of Si particles with good electrical connectivity of Ag-coating layers, giving the reduction in charge-transfer resistance.

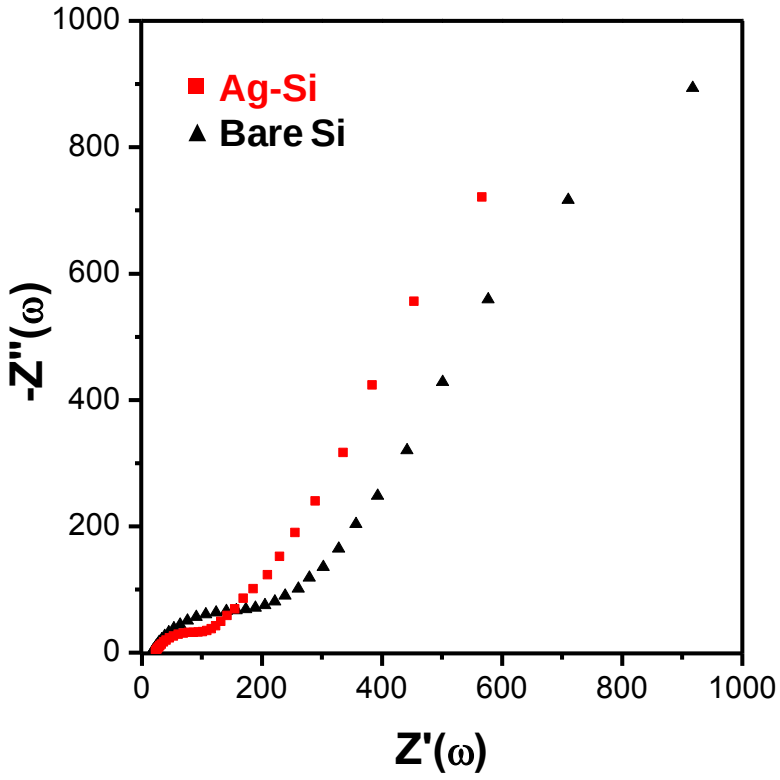

Figure 2.10. Electrochemical AC impedance spectra of bare Si (black) and Ag-coated Si (red) electrodes after 100 cycles.

2.4 Conclusion

We described a facile, but straightforward process to synthesize Ag-coated Si particles via a one-pot chemical reduction process at low temperature. The uniformly Ag-coated layers on the Si surface were electrically conductive and Ag particle size and surface coverage could be controllable. Also, the highly dispersive Ag-coated Si particles and the significant conductivity enhancement of Si led to markedly improved electrochemical performances, including a high reversible capacity, a superior cycling life, and excellent rate capabilities in lithium-ion batteries. This simple chemical reduction process can be extended to other metal and/or metal oxide materials to synthesize high-performance anode materials for practical battery applications.

2.5 References

1. Nazri, G.-A.; Pistoia, G., *Lithium Batteries: Science and Technology*. Kluwer Academic/ Plenum : 2004.
2. Tarascon, J.-M.; Armand, M., Issues and challenges facing rechargeable lithium batteries. *Nature* **2001**, 414 (6861), 359-367.
3. Song, M.-K.; Park, S.; Alamgir, F. M., Cho, J., Liu, M., Nanostructured electrodes for lithium-ion and lithium-air batteries: the latest developments, challenges, and perspectives. *Materials Science and Engineering: R* **2011**, 72, 203-252.
4. Mukherjee, R.; Krishnan, R.; Lu, t.-M.; Koratkar, N., Nanostructured electrodes for high-power lithium ion batteries. *Nano Energy* **2012**, 1, 518-533.
5. Liu, C.; Li, F.; Ma, L.-P.; Cheng, H.-M., Advanced Materials for Energy Storage. *Advanced Materials* **2010**, 22, E28-E62H.
6. Wu, H.; Cui, Y., Designing nanostructured Si anodes for high energy lithium ion batteries. *Nano Today* **2012**, 7, 414-429.
7. Kim, M. G.; Cho, J., Reversible and High-Capacity Nanostructured Electrode Materials for Li-Ion Batteries. *Advanced Functional Materials* **2009**, 19, 1497-1514.
8. Li, J.; Dahn, J. R., An In Situ X-Ray Diffraction Study of the Reaction of Li with Crystalline Si. *Journal of The Electrochemical Society* **2007**, 154, A156-A161.
9. Obrovac, M. N.; Krause, L. J., Reversible Cycling of Crystalline Silicon Powder. *Journal of The Electrochemical Society* **2007**, 154, A103-A108.
10. Kasavajjula, U.; Wang, C.; Appleby A. J., Nano- and bulk-silicon-based insertion anodes for lithium-ion secondary cells. *Journal of Power Sources* **2007**, 163, 1003-1039.
11. Chan, C. K.; Peng, H. L.; Li,u G.; McIlwrath, K.; Zhang, X. F.; Huggins, R. A.; Cui, Y., High-performance lithium battery anodes using silicon nanowires. *Nature Nanotechnology* **2008**, 3, 31-35.
12. Magasinski, A.; Dixon, P.; Hertzberg, B.; Kvit, A.; Ayala, J.; Yushin, G., High-performance lithium-ion anodes using a hierarchical bottom-up approach. *Nature Materials* **2010**, 9, 353-358.
13. Kim, H.; Seo, M.; Park, M. H.; Cho, J., A Critical Size of Silicon Nano-Anodes for Lithium Rechargeable Batteries. *Angewandte Chemie International Edition* **2010**, 49, 2146-2149.
14. Bang, B. M.; Kim, H.; Song, H.-K.; Cho, J.; Park, S., Scalable approach to multi-dimensional bulk Si anodes via metal-assisted chemical etching. *Energy & Environmental Science* **2011**, 4, 5013-5019.
15. Bruce, P. G.; Scrosati, B.; Tarascon, J.-M., Nanomaterials for Rechargeable Lithium Batteries. *Angewandte Chemie International Edition* **2008**, 47, 2930-2946.

16. Manthiram, A.; Vadivel Murugan, A.; Sarkar, A.; Muraliganth, T., Nanostructured electrode materials for electrochemical energy storage and conversion. *Energy & Environmental Science* **2008**, 1, 621-638.
17. Hu, Y.-S.; Adelhelm, P.; Smarsly, B. M.; Maier J., Highly Stable Lithium Storage Performance in a Porous Carbon/Silicon Nanocomposite. *ChemSusChem* **2010**, 3, 231-235.
18. Guo, J. C.; Chen, X. L.; Wnag, C. S., Carbon scaffold structured silicon anodes for lithium-ion batteries. *Journal of Materials Chemistry* **2010**, 20, 5035-5040.
19. Kim, H.; Han, B.; Choo, J.; Cho, J., Three-Dimensional Porous Silicon Particles for Use in High-Performance Lithium Secondary Batteries. *Angewandte Chemie International Edition* **2008**, 47, 10151-10154.
20. Park, M.-H.; Kim, M. G.; Joo, J.; Kim, K.; Kim, J.; Ahn, S.; Cui, Y.; Cho, J., Silicon Nanotube Battery Anodes. *Nano Letters* **2009**, 9, 3844-3847.
21. Ma, H.; Cheng, F.; Chen, J.-Y.; Zhao, J.-Z.; Li, C.-S.; Tao, Z.-L.; Liang, J., Nest-like Silicon Nanospheres for High-Capacity Lithium Storage. *Advanced Materials* **2007**, 19, 4067-4070.
22. Wu, H.; Chan, G.; Choi, J.W.; Ryu, I.; Yao, Y.; McDowell, M. T.; Lee, S.W.; Jackson, A.; Yang, Y.; Hu, L.B.; Cui, Y., Stable cycling of double-walled silicon nanotube battery anodes through solid–electrolyte interphase control. *Naure Nanotechnology* **2012**, 7, 309-314.
23. Hu, Y.-S.; Demir-Cakan, R.; Titirici, M.-M.; Müller, J.-O.; Schlögl, R.; Antonietti, M.; Maier, J., Superior Storage Performance of a Si@SiO_x/C Nanocomposite as Anode Material for Lithium-Ion Batteries. *Angewandte Chemie International Edition* **2008**, 47, 1645-1649.
24. Nguyen, H. T.; Zamfir, M. R.; Duong, L. D.; Lee, Y. H.; Bondavalli, P.; Pribat, D., Alumina-coated silicon-based nanowire arrays for high quality Li-ion battery anodes. *Journal of Materials Chemistry* **2012**, 22, 24618-24626.
25. Yao, Y.; Liu, N.; McDowell, M. T.; Pasta, M.; Cui, Y., Improving the cycling stability of silicon nanowire anodes with conducting polymer coatings. *Energy & Environmental Science* **2012**, 5, 7927-7930.
26. Yoo, H.; Lee, J.-I.; Kim, H.; Lee, J.-P.; Cho, J.; Park, S., Helical Silicon/Silicon Oxide Core-Shell Anodes Grown onto the Surface of Bulk Silicon. *Nano Letters* **2011**, 11, 4324-4328.
27. Guo, Y.-G.; Hu, Y.-S.; Sigle, W.; Maier, J., Superior Electrode Performance of Nanostructured Mesoporous TiO_2 (Anatase) through Efficient Hierarchical Mixed Conducting Networks. *Advanced Materials* **2007**, 19, 2087-2091.
28. Murugesan, S.; Harris, J. T.; Korgel, B. A.; Stevenson, K. J., Copper-Coated Amorphous Silicon Particles as an Anode Material for Lithium-Ion Batteries. *Chemistry of Materials* **2012**, 24, 1306-1315.
29. Yang, X. L.; Wen, Z. Y.; Huang, S. H.; Zhu, X. J.; Zhang, X. F., Electrochemical performances of silicon electrode with silver additives. *Solid State Ionics* **2006**, 177, 2807-2810.

30. Kim, J. W.; Ryu, J. H.; Lee, K. T.; Oh, S. M., Improvement of silicon powder negative electrodes by copper electroless deposition for lithium secondary batteries. *Journal of Power Sources* **2005**, 147, 227-233.
31. Chen, D.; Mei, X.; Ji, G.; Lu, M.; Xie, J.; Lu, J.; Lee, J. Y., Reversible Lithium-Ion Storage in Silver-Treated Nanoscale Hollow Porous Silicon Particles. *Angewandte Chemie International Edition* **2012**, 51, 2409-2413.
32. Yu, Y.; Gu, L.; Zhu, C.; Tsukimoto, S.; Aken, P. A. van; Maier, J., Reversible Storage of Lithium in Silver-Coated Three-Dimensional Macroporous Silicon. *Advanced Materials* **2010**, 22, 2247-2250.
33. Chen, H.; Xiao, Y.; Wang, L.; Yang, Y., Silicon nanowires coated with copper layer as anode materials for lithium-ion batteries. *Journal of Power Sources* **2011**, 196, 6657-6662.
34. Yang, X.; Wen, Z.; Huang, S.; Zhu, X.; Zhang, X., Electrochemical performances of silicon electrode with silver additives. *Solid State Ionics* **2006**, 177, 2807-2810.
35. Culity, B. D., *Elements of X-Ray Diffraction*. Addison-Wesley : 1978.
36. Park, H. K.; Yoon, J. K.; Kim, K., Novel Fabrication of Ag Thin Film on Glass for Efficient Surface-Enhanced Raman Scattering. *Langmuir* **2006**, 22, 1626-1629.
37. Kim, K.; Kim, H. S.; Park, H. K., Facile Method To Prepare Surface-Enhanced-Raman-Scattering-Active Ag Nanostructures on Silica Spheres. *Langmuir* **2006**, 22, 8083-8088.
38. Morales, J.; Sánchez, L.; Martin, F.; Ramos-Barrado, J. R.; Sánchez, M., Synthesis, Characterization, and Electrochemical Properties of Nanocrystalline Silver Thin Films Obtained by Spray Pyrolysis. *Journal of The Electrochemical Society* **2004**, 151, A151-A157.
39. Liu, W.-R.; Wang, J.-H.; Wu, H.-C.; Shieh, D.-T.; Yang, M.-H.; Wu, N.-L., Electrochemical Characterizations on Si and C-Coated Si Particle Electrodes for Lithium-Ion Batteries. *Journal of The Electrochemical Society* **2005**, 152, A1719-A1725.
40. Esmanski, A.; Ozin, G. A., Silicon Inverse-Opal-Based Macroporous Materials as Negative Electrodes for Lithium Ion Batteries. *Advanced Functional Materials* **2009**, 19, 1999-2010.
41. Liu, X. H.; Zhong, L.; Huang, S.; Mao, S. X.; Zhu, T.; Huang, J. Y., Size-Dependent Fracture of Silicon Nanoparticles During Lithiation. *ACS Nano* **2012**, 6, 1522-1531.

III. Synthesis of antimony-doped tin oxide coated natural graphite and its electrochemical property as battery anode

3.1 Introduction

Currently, lithium-ion batteries (LIBs) have attracted much attention as energy storage devices owing to their high energy and high power density, light weight, and environmental safety.[1] Among many anode materials, natural graphite is a standard material due to its high reversibility, small volume change and low cost. However, since large size energy storage systems have been required for electric vehicles (EVs) and smart grids,[2-6] limited capacity (372 mA h g^{-1}) of graphite has been problems concerning high-energy density applications.[7-8] Therefore, many researchers have studied to develop anode materials which exhibit a high capacity, a long cycling life and an excellent high rate performance.

Various strategies have been developed including carbon-based materials,[9] polymers,[10] metal oxides, [11-16], and their composites.[17-20] Among them, SnO_2 has been considered as a potential anode owing to its higher theoretical specific capacity of 790 mAh g^{-1} and reasonable discharge potential (<1.5 V). However, its large volume expansion and severe aggregation during the Li^+ insertion and extraction leads to pulverization and loss of capacity.[21-26] To solve these problems, antimony (Sb) particles are doped within the SnO_2 particles (denoted as ATO), in which Sb is a common n-type dopant in SnO_2. The concentration of free electrons in SnO_2 significantly increases after Sb doping, so that the ATO exhibits high electrical conductivity and high optical transmission. With these advantages, ATO has been attracted much attention to numerous applications, such as transparent electrodes, displays, electrochromic windows, rechargeable LIBs, and energy storage devices.[27-29]

In this paper, we describe synthesis of new type of graphite composite whose surface is homogenously covered with ATO nanoparticles. The as-synthesized ATO-graphite composite exhibits significantly improved electrochemical performances including a high specific reversible capacity, highly stable cycling property, and excellent rate capability, compared to pristine graphite.

3.2 Experimental

3.2.1 Synthesis of ATO-coated graphite

1.5 g of natural graphite powder was put into a hydrogen peroxide (H_2O_2, 34.5 wt%, SAMCHUN Chemical), and the mixture was stirred at 50 °C for 30 minutes to activate the surface of graphite. Subsequently, the natural graphite was separated by a centrifugation and dried at 80 °C in a vacuum oven. Then, 0.25-1.5 g of ATO colloidal solution (an average particle size = 20 nm, solid content = 30 wt% in methanol, FNC CHEM Co.) was added to the 5 mL of methanol (>99.9 %, Aldrich) and 1.5g of activated natural graphite was added with stirring for 2 hr. Also, citric acid (Aldrich) was added to the mixture of ATO and graphite to coat ATO on the graphite more uniformly and to use as a carbon source. After the sufficient stirring, the mixture was dried at 80 °C in a vacuum oven to remove the methanol completely. The dried sample was heated to 400 °C at a speed of 2 °C min^{-1} for 5 h in air.

3.2.2 Characterization of ATO-coated graphite

Surface morphologies of pristine graphite and ATO-coated graphite were characterized by a scanning electron microscopy (SEM, Nano SEM 230, FEI) operating at 10 kV. The microstructure of both graphite particles were analyzed from high power X-ray diffractometer (Rigaku D/MAX) at 2500 V between 10° and 80° at a scan rate of 2° min^{-1}. The elemental analysis (EA) was performed in order to investigate the contents of ATO nanoparticles on the graphite surface.

3.2.3 Electrochemical tests

The electrochemical properties of pristine graphite and ATO-coated graphite electrodes were tested by galvanostatic discharging and charging in coin-type half cells (2016 R-type). The cells that were composed of active material/super P carbon black/binder composite as a working electrode and lithium metal as a counter electrode, were prepared in an argon-filled glove box. The electrode was composed of active material (pristine graphite or ATO-coated graphite, 90 wt%), super P carbon black (2 wt%), and poly(acrylic acid)/sodium carboxymethyl cellulose (50/50 wt%/wt%, Aldrich) binder (8 wt%). The resulting slurry was coated on a Cu current collector and dried in a vacuum oven at 150 °C for 2 hr. The electrolyte was composed of 1.3M $LiPF_6$ in ethylene carbonate/diethyl carbonate (EC/DEC, 30/70 v/v, Panaxetec) with 10 wt% fluoroethylene carbonate (FEC). The cells were cycled at a rate of 0.2-5 C between 0.005-3 V (vs. Li/Li^+). All electrochemical measurements were carried out with a WBCS-3000 battery cycler (Wonatech Co.) at room temperature.

3.3 Results and discussion

We developed a facile synthetic process to produce the ATO nanoparticles-based surface modification of graphite materials, denoted as ATO-NG. Schematic illustration describes synthetic routes of ATO-NG materials (Figure 3.1). Typically, because the surface of natural graphite is very hydrophobic, it is hard to modify the surface with other materials. For this reason, the natural graphite was activated to improve the reactivity with different material. The graphite powders were put into a hydrogen peroxide at 50 ^{o}C with 30 min stirring. Then, 0.5 g of 30 wt% ATO colloidal solution was added to the 5 mL of methanol and 1.5g of activated graphite was added subsequently with 2 hr stirring. Owing to the good dispersion of ATO nanoparticles in methanol, the graphite particles were compatible with the ATO colloids. After 2 hr, the mixture was dried to remove the solvent completely and heated at 400 ^{o}C for 5 hr under air atmosphere to make ATO-encapsulated natural graphite.

SEM images in Figure 3.1 shows the surface morphologies of the ATO-NG particles. To investigate the effect of surface activation of graphite, two samples were prepared; one is non-activated natural graphite and the other is activated natural graphite. The pristine graphite (Figure 3.1.a & 3.1.b) showed smooth planes with the size of around 20 μm. The ATO-NG using non-activated graphite (Figure 3.1.c & 3.1.d) exhibited small amount of ATO nanoparticles. In contrast, activated natural graphite (Figure 3.1.e & 3.1.f) showed ATO-NG particles decorated with large amount of ATO particles. It should be noted that the surface of graphite was changed from hydrophobic to hydrophilic through the activation process, so that ATO nanoparticles could be easily deposited on the graphite surface.

To confirm the ATO nanoparticles, we obtained XRD patterns of pristine graphite and ATO-NG particles (Figure 3.2). The XRD patterns of pristine graphite showed a pure graphite (JCPDS Card no. 23-0064), while the ATO-NG showed new peaks which are in good agreement with the reflections of cassiterite SnO_2 (JCPDS Card no. 21-1250). Meanwhile, antimony (Sb) doping made shift of peak positions a little, indicating that Sb is cooperated into the SnO_2 lattice to form the ATO solid solution.[30-31]

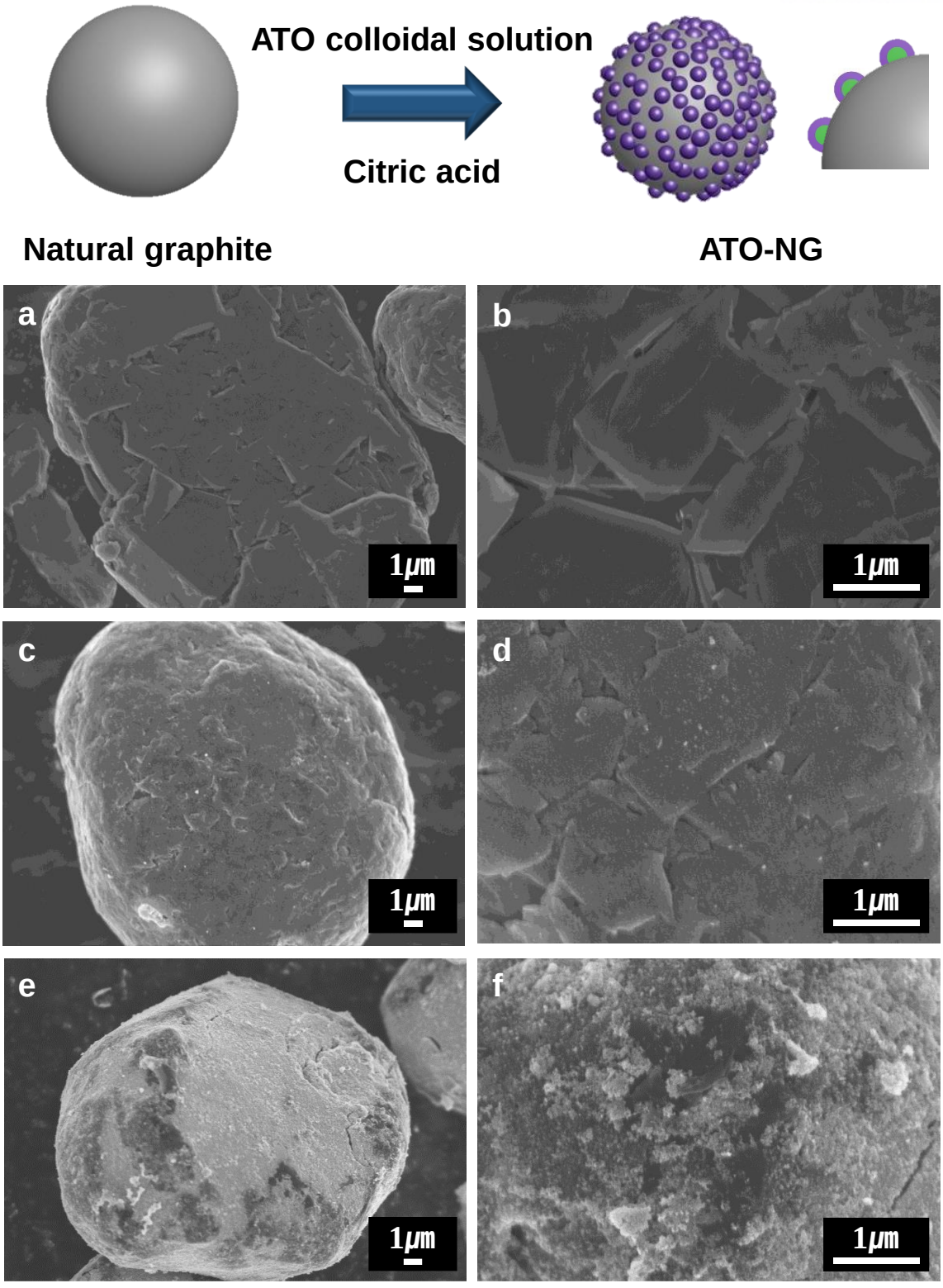

Figure 3.1. Top: schematic illustration showing synthetic process of ATO-NG. Bottom: SEM images of (a) and (b) bare natural graphite, (c) and (d) ATO-$NG_{1:10}$ using non-activated NG, (e) and (f) ATO-$NG_{1:10}$ using activated NG.

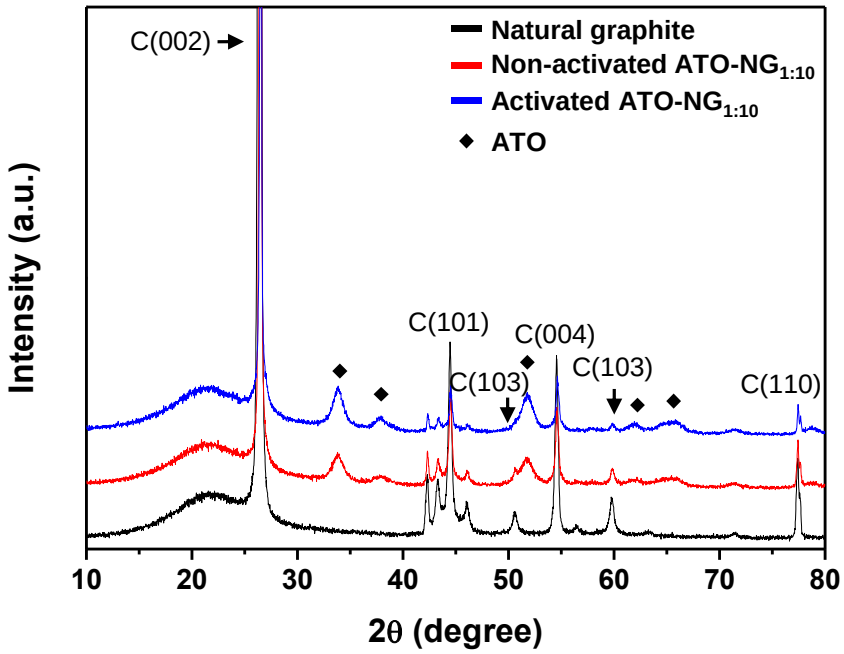

Figure 3.2. XRD patterns of bare natural graphite (black), ATO-$NG_{1:10}$ using non-activated NG (red), and ATO-coated $graphite_{1:10}$ using activated (blue).

The surface coverage of ATO nanoparticles on the graphite surface can be tuned by controlling the amount of ATO colloidal solution. We synthesized three samples with different ratio of natural graphite to ATO nanoparticles. When 1.5 g of natural graphite reacted with 0.25 g (0.075 g of pure ATO, ATO-$NG_{1:20}$), 0.5 g (0.15 g of pure ATO, ATO-$NG_{1:10}$), and 1.5 g (0.45 g of pure ATO, ATO-$NG_{3:10}$) of ATO colloidal solution, the increasing amount of ATO nanoparticles showed higher surface coverage to the graphite (Figure 3.3). The SEM images in Figure 3.3 show various surface morphologies of ATO-NG particles. The ATO-$NG_{1:20}$ (Figure 3.3.a & 3.3.b) looked like no ATO nanoparticles on the graphite surface in a low magnification due to small amount of ATO. However, ATO nanoparticles were observed in a high magnification. The ATO-$NG_{1:10}$ was clearly seen in the SEM image (Figure 3.3.c & 3.3.d). In case of the ATO-$NG_{3:10}$, more densely covered ATO nanoparticles were seen on the graphite surface (Figure 3.3.e & 3.3.f). However, non-uniformly coated ATO and serious aggregated ATO were observed on the graphite surface. From these results, we can say that the optimum condition is ATO-$NG_{1:10}$.

The XRD patterns of three ATO-NG samples were analyzed to confirm the ATO nanoparticles (Figure 3.4). All samples showed typical peaks of natural graphite and ATO nanoparticles, and no other peaks were existed.

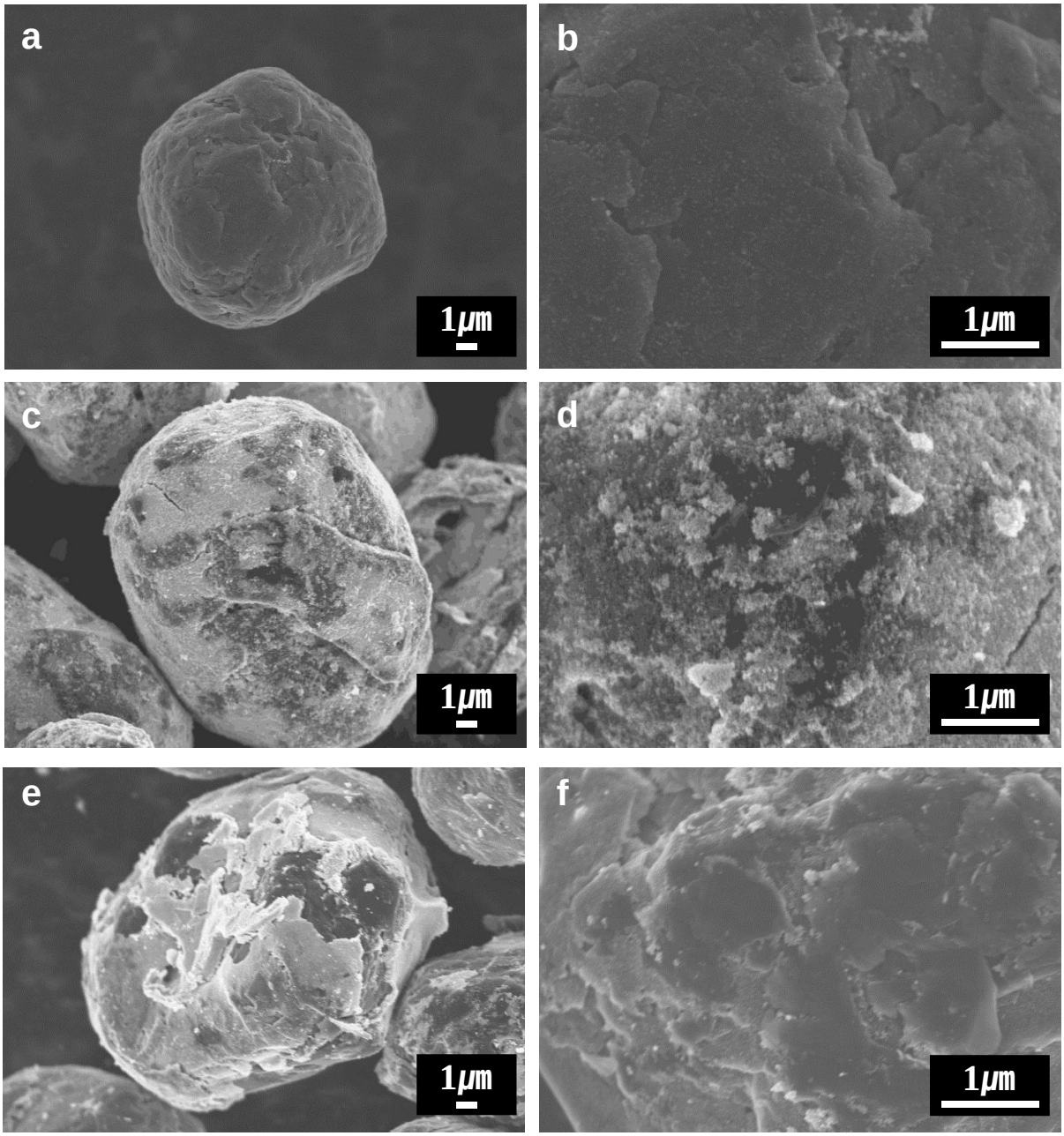

Figure 3.3. SEM images of (a) and (b) ATO-$NG_{1:20}$, (c) and (d) ATO-$NG_{1:10}$, (e) and (f) ATO-$NG_{3:10}$.

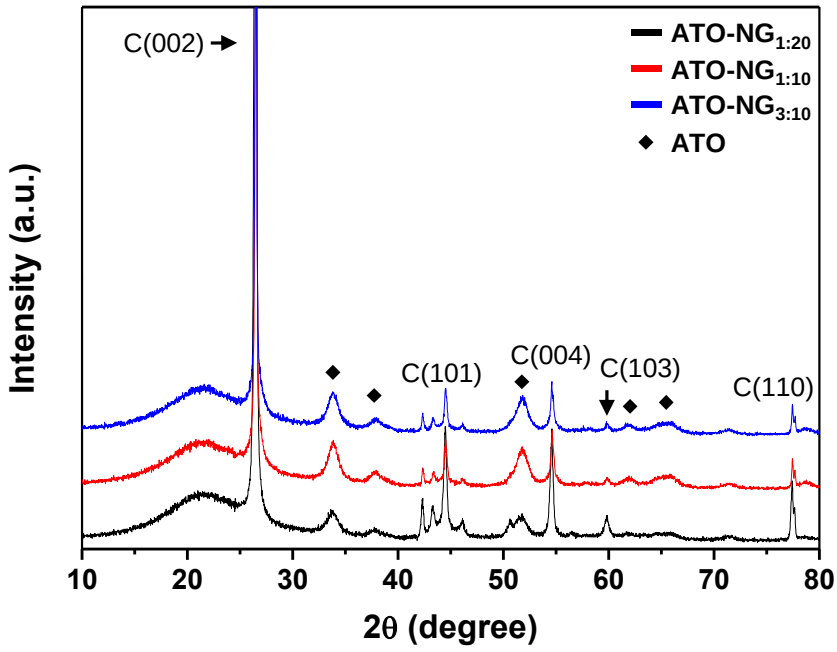

Figure 3.4. XRD patterns of ATO-$NG_{1:20}$ (black), ATO-$NG_{1:10}$ (red), and ATO-$NG_{3:10}$ (blue).

Numerous studies on the modification of natural graphite have been reported including mild oxidation, metals or metal oxides deposition, polymer coating, carbon coating, and so on.[8] Especially, carbon coating process has been used with several advantages, such as increasing the electrical conductivity and forming a stable solid-electrolyte interface (SEI) layer.[32-33]

To use of several advantages of carbon layers, we modified synthetic routes mentioned above. When citric acid, which acts as a carbon precursor, was added to the mixture of ATO colloidal solution and activated graphite. Since the solubility of pure citric acid in alcohol is quite high, citric acid is dispersed well in ATO nanoparticle-dispersed methanol. Subsequent process is the same as that of ATO-NG synthesis. Only different thing is that the citric acid evaporates at 400 ^{o}C in air, and then changed to inert Ar atmosphere in order to carbonize the citric acid. The surface morphologies of ATO-coated graphite were shown in Figure 3.5. SEM images of ATO-$NG_{1:20}$ with carbon layers (Figure 3.5.a and 3.5.b) and ATO-$NG_{1:10}$ with carbon layers (Figure 3.5.c and 3.5.d) show that more uniformly coated ATO nanoparticles are obtained by introduction of citric acid. Also, we confirmed that carbon coating process was not change the microstructure of ATO nanoparticles by XRD patterns (Figure 3.6).

To investigate the contents of ATO nanoparticles, the element analysis (EA) was performed; the ratio of ATO nanoparticles to natural graphite=1:10 was fixed (Figure 3.7). Among several samples, ATO-$NG_{1:10}$ using non-activated graphite and without carbon coating (Figure 3.7.a) had a smallest ATO contents due to the poor reactivity between ATO nanoparticles and graphite, compared to ATO-$NG_{1:10}$ using activated graphite without carbon coating (Figure 3.7.b) and non-activated graphite with carbon coating (Figure 3.7.c). These results showed similar contents of ATO particles, indicating that ATO nanoparticles should be coated well on the graphite surface. As expected, large amount of ATO nanoparticles were detected in the ATO-$NG_{1:10}$ using activated graphite with carbon coating (Figure 3.7.d).

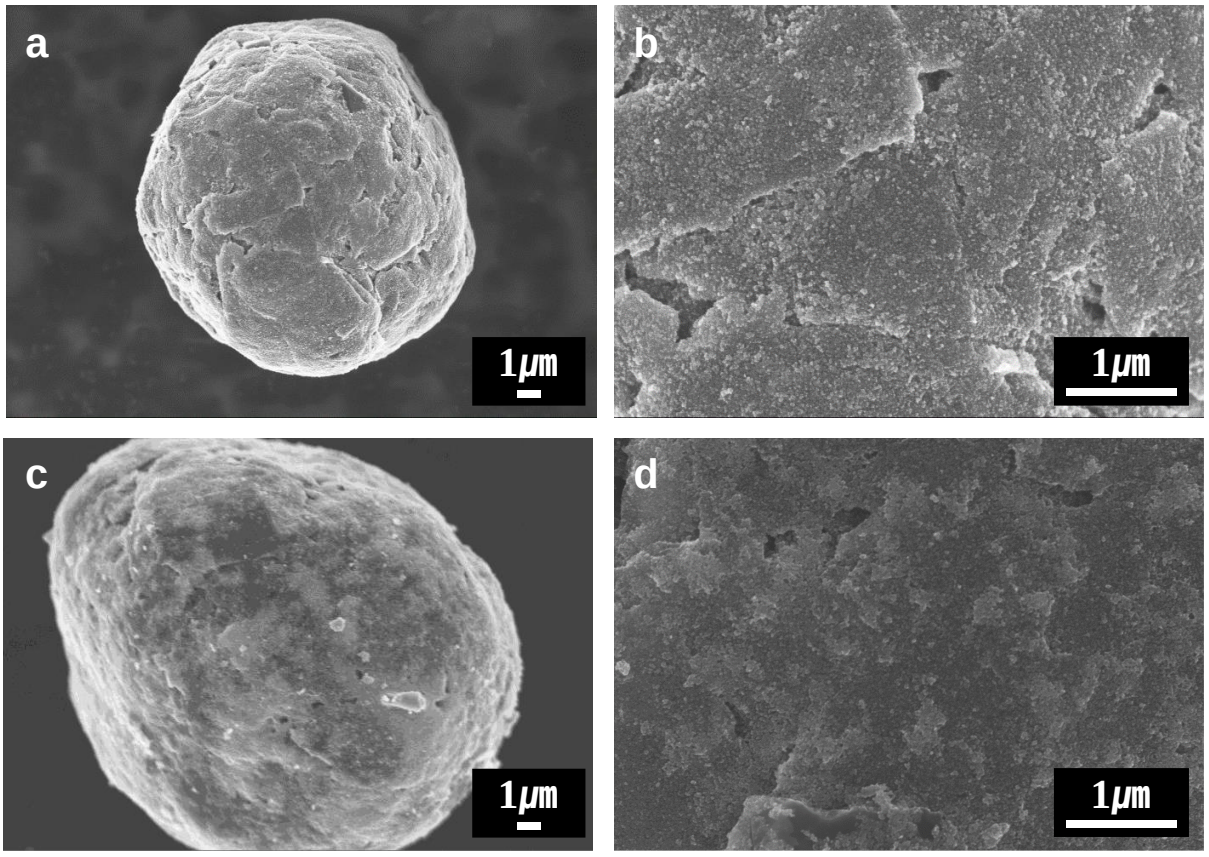

Figure 3.5. SEM images of (a) and (b) ATO-$NG_{1:20}$ with carbon coating, (c) and (d) ATO-$NG_{1:10}$ with carbon coating.

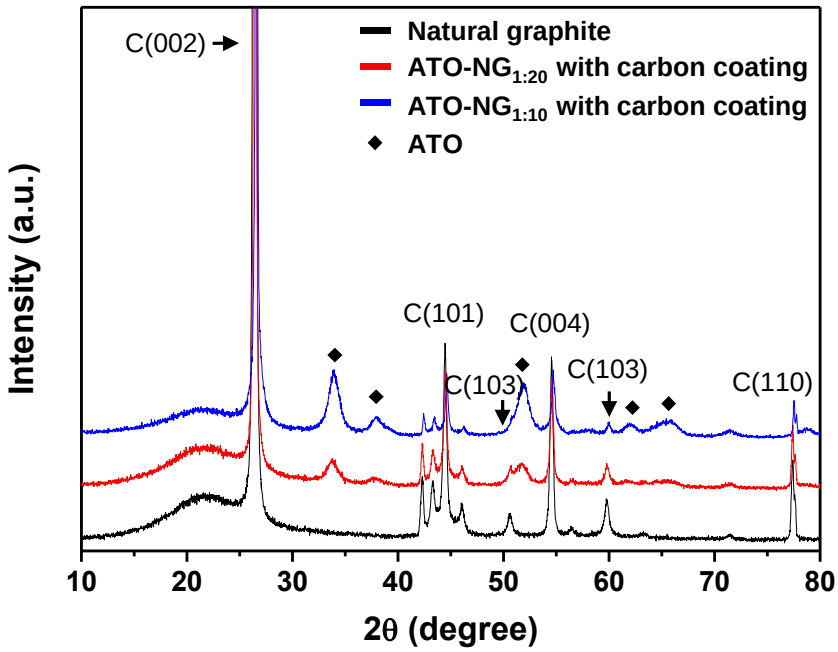

Figure 3.6. XRD patterns of bare natural graphite (black), ATO-$NG_{1:20}$ with carbon coating (red), and ATO-$NG_{1:10}$ with carbon coating (blue).

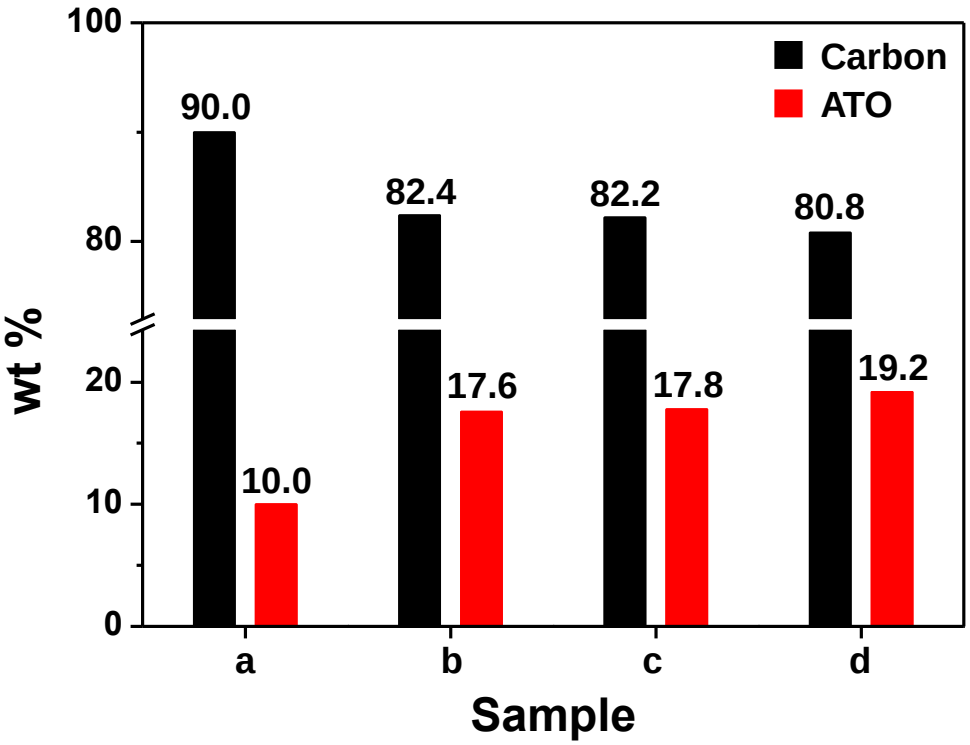

Figure 3.7. Elemental analysis (EA) of ATO-NG. The amount of ATO colloidal solution was fixed to 0.5 g: Without carbon coating using (a) non-activated graphite and (b) activated-graphite, and with carbon coating using (c) non-activated graphite and (d) activated graphite.

The electrochemical properties of pristine graphite and three different ATO-NG particles were tested by galvanostatic discharging and charging using a coin-type half cell (2016R) within 0.005-3.0 V (vs. Li/Li^+). Figure 3.8.a shows the first voltage profiles of all electrodes at 0.2 C rate. ATO-$NG_{1:20}$ showed discharge (lithiation) and charge (delithiation) capacities are 432 and 380 mAh g^{-1}, respectively, and the ATO-$NG_{1:10}$ has a discharge (charge) capacities of 475 (399) mAh g^{-1}. In particular, ATO-$NG_{1:10}$ with carbon layers exhibits an enhanced discharge capacity of 533 mAh g^{-1} and charge capacity of 460 mAh g^{-1}, corresponding to an initial coulombic efficiency of 83%. We can explain the increasing capacity as follows: ATO nanoparticles are deposited easily and uniformly on the graphite surface through carbon coating process, so that ATO-$NG_{1:10}$ with carbon layers show the highest contents of ATO (Figure 3.7). In this case, approximately 20wt% ATO nanoparticles contributed to the specific capacity. Theoretical capacity of graphite is 372 mAh g^{-1}, while ATO exhibits 1500 mAh g^{-1}.[34]

Figure 3.8.b shows the cycling performance of all samples at 0.5 C rate. The natural graphite exhibits low charge capacity of 277 mAh g^{-1} after 50 cycles, corresponding to the capacity retention of 87% compared to initial capacity. Meanwhile, the ATO-$NG_{1:10}$ with carbon layers exhibits the charge capacity of 394 mAh g^{-1} after 50 cycles, with a capacity retention of 86%. All ATO-NG electrodes show stable cycle retention, because ATO nanoparticles can also enhance the electrical conductivity.[35]

The rate capabilities of electrodes are plotted in Figure 3.9. The natural graphite shows a significant capacity drop at 3 C rate and a specific capacity of only 43% at 5 C compared to the capacity at 0.2 C rate. In contrast, ATO-$NG_{1:10}$ with carbon layers showed outstanding rate capability until a high rate of 5 C, with a specific capacity of 81 % at 5 C compared to 0.2 C. This result indicates that uniformly coated ATO particles leads to a significant enhancement in the electrical conductivity, resulting in superior electrochemical properties.

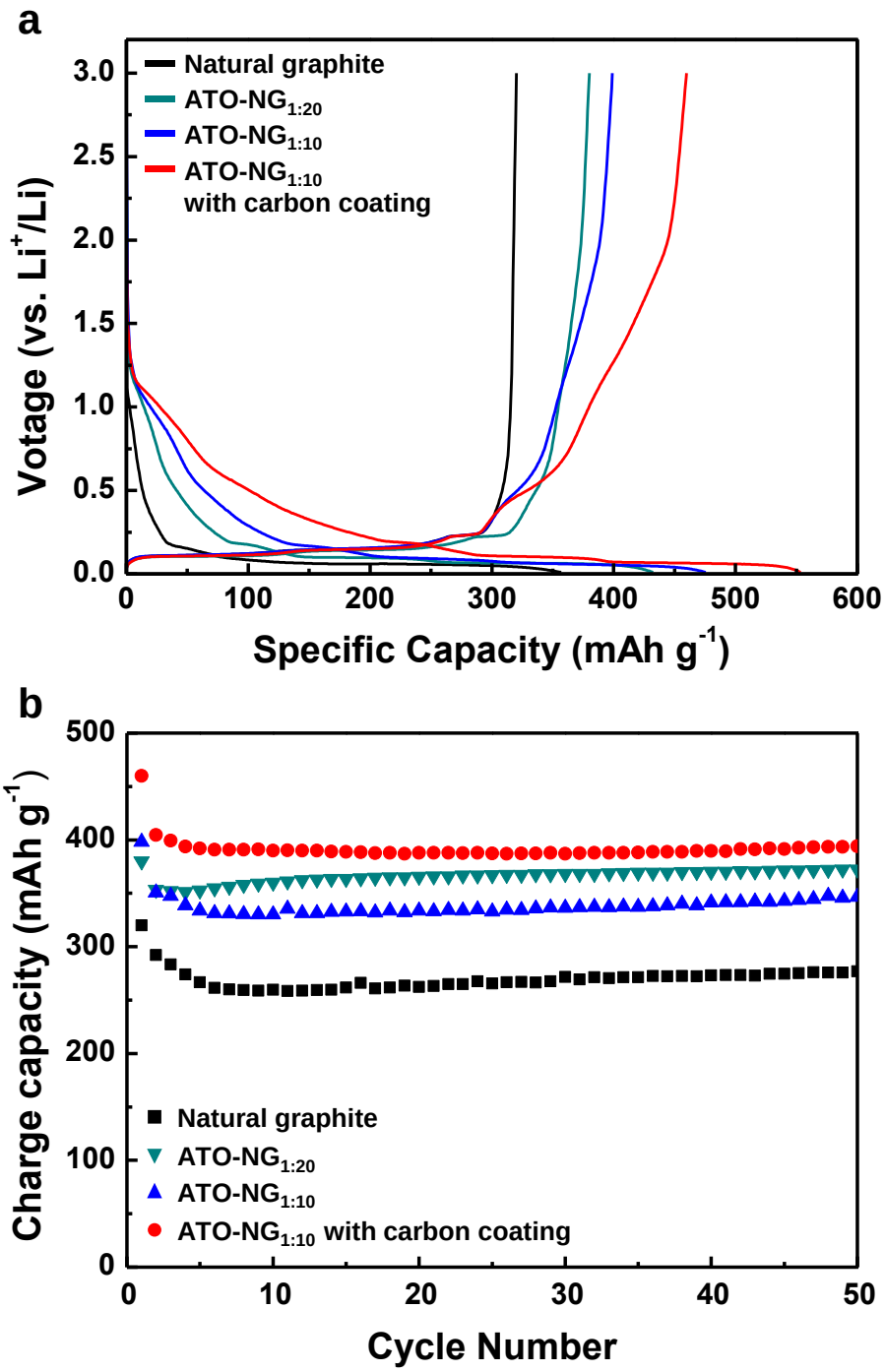

Figure 3.8. Electrochemical performances of bare natural graphite and ATO-coated graphite electrodes: (a) First cycle at 0.05 C in the range of 0.005-3 V and (b) cycling performance of bare natural graphite and ATO-coated graphite electrodes.

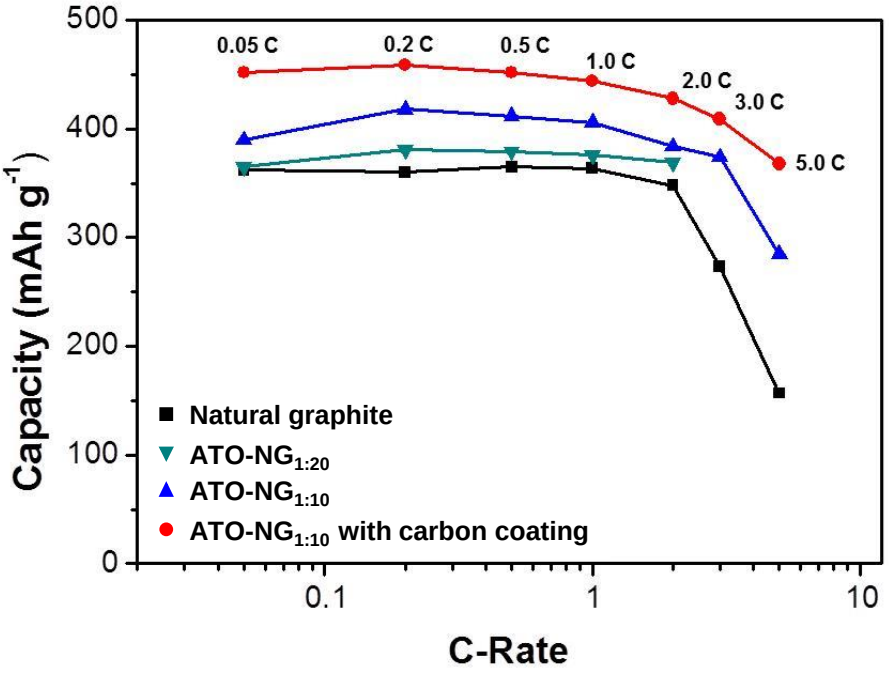

Figure 3.9. Rate capabilities (0.2-5 C) of bare natural graphite and ATO-NG electrodes.

3.4 Conclusion

In summary, we described a simple process to synthesize ATO-coated graphite particles. The ATO nanoparticles were deposited on the graphite surface via a heat treatment and the surface coverage could be tuned by controlling of the amount of ATO colloidal solution. In order to coat a more uniform ATO layers, the carbon coating process of ATO-NG was introduced using carbon source. The ATO-coated graphite particles considerably improved electrochemical performances, including a high reversible capacity, a superior cycling life, and an excellent rate capability in LIBs, because the ATO nanoparticles on the graphite surface contributed to increase specific capacity and electronic conductivity. This strategy can be extended to other materials to synthesize advanced anode and cathode materials for practical LIB applications.

3.5 References

1. Park, J.-K., *Principles and Applications of Lithium Secondary Batteries*. Wiley-VCH Verlag GmbH & Co. KGaA : 2012.
2. Choi, N.-S.; Chen, Z.; Freunberger, S. A.; Ji, X.; Sun, Y.-K.; Amine, K.; Yushin, G.; Nazar, L. F.; Cho, J.; Bruce, P. G., Challenges Facing Lithium Batteries and Electrical Double-Layer Capacitors. *Angewandte Chemie International Edition* **2012**, 51 (40), 9994-10024.
3. Megahed, S.; Scrosati, B., Lithium-ion rechargeable batteries. *Journal of Power Sources* **1994**, 51 (1), 79-104.
4. Etacheri, V.; Marom, R.; Elazari, R.; Salitra, G.; Aurbach, D., Challenges in the development of advanced Li-ion batteries: a review. *Energy & Environmental Science*, **2011**, 4 (9), 3243-3262
5. Nishi, Y., Lithium ion secondary batteries; past 10 years and the future. *Journal of Power Sources* **2001**, 100 (1), 101-106.
6. Dunn, B.; Kamath, H.; Tarascon, J. M., Electrical Energy Storage for the Grid: A Battery of Choices. *Science*, **2011**, 334, 928-935
7. Buqa, H.; Goers, D.; Holzapfel M.; Spahr M. E.; Novák P., High Rate Capability of Graphite Negative Electrodes for Lithium-ion Batteries. *J. Electrochem. Soc.* **2005**, 152 (2), A474-A481.
8. Wu, Y.P.; Rahm, E.; Holze, R., Carbon anode materials for lithium ion batteries. *Journal of Power Sources* **2003**, 114, 228-236.
9. Guo, P.; Song, H.; Chen, X., Electrochemical performance of graphene nanosheets as anode material for lithium-ion batteries. *Electrochemistry Communications* **2009**, 11 (6), 1320-1324.
10. Kumai, Y.; Shirai, S.; Sudo, E.; Seki, J.; Okamoto H.; Sugiyama Y.; Nakano H., Characteristics and structural change of layered polysilane (Si_6H_6) anode for lithium ion batteries. *Journal of Power Sources* **2011**, 196 (3), 1503-1507.
11. Yong, C.; Shuang, L.; Xiaoming, Y.; Quanyi, H.; Ming, Z.; Taihong, W., Facile preparation of porous one-dimensional Mn_2O_3 nanostructures and their application as anode materials for lithium-ion batteries. *Physica E* **2010**, 43, 70-75.
12. Cui, Z.-M.; Hang, L.-Y.; Song, W.-G.; Guo, Y.-G., High-Yield Gas-Liquid Interfacial Synthesis of Highly Dispersed Fe_3O_4 Nanocrystals and Their Application in Lithium-Ion Batteries. *Chemistry of Materials* **2009**, 21 (6), 1162-1166.
13. Li, L.M.; Yin, X.; Liu, S.; Wang, Y.; Chen, L; Wang, T., Electrospun porous SnO_2 nanotubes as high capacity anode materials for lithium ion batteries. *Electrochemistry Communications* **2010**, 12 (10), 1383-1386.
14. Pfanzelt, M.; Kubiak, P.; Fleischhammer, M.; Wohlfahrt-Mehrens, M., TiO_2 rutile-An alternative anode material for safe lithium-ion batteries. *Journal of Power Sources* **2011**, 196

(16), 6815-6821.

15. Huang, X.H.; Xia, X.H.; Yuan, Y.F.; Zhou, F., Porous ZnO nanosheets grown on copper substrates as anodes for lithium ion batteries. *Electrochimica. Acta* **2011**, 56 (14), 4960-4965.
16. Li, Y.; Tan, B.; Wu, Y., Mesoporous Co_3O_4 Nanowire Arrays for Lithium Ion Batteries with High Capacity and Rate Capability. *Nano Letters* **2008**, 8 (1), 265–270.
17. Wu, Z.-S.; Ren, W.; Wen, L.; Gao, L.; Zhao, J.; Chen, Z.; Zhou, G.; Li, F.; Cheng, H.-M., Graphene Anchored with Co_3O_4 Nanoparticles as Anode of Lithium Ion Batteries with Enhanced Reversible Capacity and Cyclic Performance. *ACS Nano* **2010**, 4 (6), 3187-3194.
18. Wang, X.; Zhou, X.; Yao, K.; Zhang, J.; Liu Z., A SnO_2/graphene composite as a high stability electrode for lithium ion batteries. *Carbon* **2011**, 49 (1), 133-139.
19. Xing, L.; Cui, C.; Ma, C.; Xue, X., Facile synthesis of α-MnO2/graphene nanocomposites and their high performance as lithium-ion battery anode. *Materials Letters* **2011**, 65 (14), 2104-2106.
20. Zhou G.; Wang D.W.; Li F.; Zhang L.; Li N.; Wu Z. S.; Wen L.; Lu G. Q; Cheng H. M., Graphene-Wrapped Fe_3O_4 Anode Material with Improved Reversible Capacity and Cyclic Stability for Lithium Ion Batteries. *Chemistry of Materials* **2010**, 22 (18), 5306-5313.
21. Kim, J. G.; Nam, S. H.; Lee, S. H.; Choi, S. M.; Kim, W. B., SnO_2 Nanorod-Planted Graphite: An Effective Nanostructure Configuration for Reversible Lithium Ion Storage. *ACS Applied Materials & Interfaces* **2011**, 3, 828-835.
22. Li, Y.; Zhu, S.; Liu, Q.; Gu, J.; Guo, Z.; Chen, Z.; Feng, C.; Zhang, D.; Moon, W.-J., Carbon-coated SnO_2@C with hierarchically porous structures and graphite layers inside for a high-performance lithium-ion battery. *Journal of Materials Chemistry* **2012**, 22, 2766-2773.
23. Courtney, I. A.; McKinnon, W. R.; Dahn, J. R., On the Aggregation of Tin in SnO Composite Glasses Caused by the Reversible Reaction with Lithium. *Journal of The Electrochemical Society* **1999**, 146, 59-68.
24. Poizot, P.; Laruelle, S.; Grugeon, S.; Dupont L.; Tarascon, J. M., Nano-sized transition-metaloxides as negative-electrode materials for lithium-ion batteries. *Nature* **2000**, 407, 496-499.
25. Lou, X. W.; Deng, D.; Lee, J. Y.; Feng, J.; Archer, L.A., Self-Supported Formation of Needlelike Co_3O_4 Nanotubes and Their Application as Lithium-Ion Battery Electrodes. *Advanced Materials* **2008**, 20, 258-262.
26. Ma, H.; Zhang, S.; Ji, W.; Tao, Z.; Chen, J., α-CuV_2O_6 Nanowires: Hydrothermal Synthesis and Primary Lithium Battery Application. *JACS* **2008**, 130, 5361–5367.
27. Wang, Y.; Djerdj, I.; Smarsly, B.; Antonietti, M., Antimony-Doped SnO_2 Nanopowders with High Crystallinity for Lithium-Ion Battery Electrode. *Chemistry of Materials* **2009**, 21, 3202-3209.

28. Stjerna, B.; Olsson, E.; Granqvist, C. G., Optical and electrical properties of radio frequency sputtered tin oxide films doped with oxygen vacancies. F, Sb, or Mo. *Journal of Applied Physics* **1994**, 76, 3797-3817.
29. Hu, P.; Yang, H., Controlled coating of antimony-doped tin oxide nanoparticles on kaolinite particles. *Applied Clay Science* **2010**, 48, 368-374.
30. Qin, Y.; Zhong, L.; Wu, B., Preparation of ATO Nanoparticles from a New Composite Complex Salt. *Materials Transactions* **2007**, 48 (1), 29-31.
31. Zhang, L.; Wu, J.; Chen, F.; Li, X.; Schoenung, J. M.; Shen, Q., Spark plasma sintering of antimony-doped tin oxide (ATO) nanoceramics with high density and enhanced electrical conductivity. *Journal of Asian Ceramic Societies* **2013**, 1, 114-119.
32. Kim, H.; Han, B.; Choo, J.; Cho, J., Three-Dimensional Porous Silicon Particles for Use in High-Performance Lithium Secondary Batteries. *Angewandte Chemie International Edition* **2008**, 47, 10151-10154.
33. Park, M.-H.; Kim, M. G.; Joo, J.; Kim, K.; Kim, J.; Ahn, S.; Cui, Y.; Cho, J., Silicon Nanotube Battery Anodes. *Nano Letters* **2009**, 9 (11), 3844-3847.
34. Yin, X. M.; Li, C. C.; Zhang, M.; Hao, Q. Y.; Liu, S.; Chen, L. B.; Wang T. H., One-Step Synthesis of Hierarchical SnO_2 Hollow Nanostructures via Self-Assembly for High Power Lithium Ion Batteries. *The Journal of Physical Chemistry C* **2010**, 114, 8084-8088.
35. Lee, J.-I.; Lee, E.-H., Park, J.-H.; Park, S.; Lee, S.-Y., Ultrahigh-Energy-Density Lithium-Ion Batteries Based on a High-Capacity Anode and a High-Voltage Cathode with an Electroconductive Nanoparticle Shell. *Advanced Energy Materials* **2014**, 4(8), 1301542-1301550.

Acknowledgement

2009 년 3 월, UNIST 첫 학부생으로 입학한지가 엊그제 같은데, 벌써 6 년이라는 시간이 흘렀습니다.

우선 석사 과정 동안 부족한 저에게 많은 기회를 주시고, 아낌없는 조언해주신 박수진 교수님께 진심으로 감사드립니다. 바쁘신 와중에도 논문 심사에 응해주신 이상영 교수님, 김병수 교수님께도 감사의 말씀을 드립니다.

또한 학부 인턴 동안 항상 따뜻하게 맞이해주시고, 그 이후에도 많은 조언해주신 문회리 교수님 대단히 감사합니다. 랩투어를 흔쾌히 응해주시고, 좋은 경험이 되도록 지도해 주신 김철민 교수님, Robert James Mitchell 교수님께 감사합니다.

석사 과정 동안 아낌없는 가르침과 조언으로 많은 도움주신 저희 실험실 권도형 박사님, 승민 오빠, 형민 오빠, 정인 언니, 신호 오빠께도 진심으로 감사합니다. 그리고 같이 석사 과정 생활을 하면서 많은 의지가 된 우진 오빠, 태수 오빠, 명수 오빠, 지은이 언니, 가은이 언니, 재건이에게도 정말 감사합니다. 또한 석사 과정 시작하면서 실험실 생활에 적응할 수 있도록 많은 도움주신 찬훈이 오빠와 옥지 언니께도 감사합니다.

학부생 때부터 힘들 때 버팀목이 되어주고, 잊을 수 없는 추억 남겨준 현규 오빠, 승희 언니, 종우 오빠, 재화 오빠에게도 정말 감사합니다. 그리고 항상 깊은 관심과 아낌없는 조언과 격려해준 본재 오빠에게도 진심으로 감사합니다. 기숙사 룸메이트로서 많은 즐거움과 추억 남겨준 혜진이에게도 감사합니다.

저에게 많은 도움 주시고, 지켜봐 주신 모든 분들께 진심으로 감사드리며, 평생 잊지 않도록 하겠습니다. 다시 한 번 감사드립니다.